Site symmetries, bleaching behavior, and thermal stability of hydrogenic centers in $SrF_2:Pr^{3+}$ and $CaF_2:Pr^{3+}$

K. M. Murdoch* and G. D. Jones
Department of Physics and Astronomy, University of Canterbury, PB 4800 Christchurch, New Zealand
(Received 7 May 1998)

Five multihydrogenic Pr^{3+} centers are found in both SrF_2 and CaF_2. All of these centers exhibit permanent bleaching at 10 K following optical excitation. This bleaching is caused by the migration of vibrationally excited hydrogenic ions into different lattice positions. Some of the excited centers are reoriented to produce equivalent centers. Alternatively, new centers with different excitation energies are created. All bleaching effects can be reversed by warming the whole crystal above 120 K. Laser selective excitation spectroscopy was used to measure energy levels of the $^1D_2$, $^3P_0$, $^3P_1$, and $^1I_6$ multiplets of these multihydrogenic centers. The Pr^{3+} site symmetries for all five centers were determined from the polarization behavior of their electronic transitions. This required the derivation of tables of polarization ratios for the C_{4v}, C_{2v}, and C_S symmetry groups. Models are proposed for the multihydrogenic centers and their photoproduct centers which are consistent with these Pr^{3+} site symmetries and account for the observed bleaching behavior. The $^1D_2$ fluorescence lifetimes of the centers were measured and support the models presented. The temperatures of fluorescence recovery for bleached centers and of fluorescence depletion for photoproduct centers were measured and found to be independent of the hydrogen isotope present. These temperatures were used to determine the barrier potentials which must be surmounted when centers revert to their original configurations.
[S0163-1829(98)01142-4]

I. INTRODUCTION

The multihydrogenic centers present in hydrogenated and deuterated CaF_2 and SrF_2 crystals containing rare-earth (R^{3+}) ions are noteworthy in showing varied 10 K bleaching behavior.[1] The bleaching observed is a form of spectral hole burning, in which the laser bandwidth is comparable to the inhomogeneously broadened linewidth of the absorption transition, producing a reduction in intensity over the whole line profile. Two types of polarized bleaching are distinguished.[2] In reorientational bleaching, centers are reoriented by 90° to produce equivalent centers. While the absorption lines of these reoriented centers lie within the inhomogeneously broadened absorption line, their new orientations are such that these centers are no longer excited by the linearly polarized laser beam and the fluorescence bleaches away to a residual intensity. Switching the laser polarization by 90° restores the fluorescence intensity. Photoproduct-formation bleaching produces distinct photoproduct centers with different absorption energies than the original centers. Bleaching occurs in either excitation polarization, with no fluorescence recovery on switching the laser polarization. Selective excitation of the photoproduct centers restores the original centers.

The whole gamut of polarized bleaching behavior, from purely reorientational bleaching to distinct photoproduct-formation bleaching, is exhibited by the Pr^{3+} $CS(1)$ through $CS(4)$ centers.[1] The ''C_S'' center labeling was originally introduced[1] as C_S is the Pr^{3+} site symmetry of the principal $CS(1)$ center. Because not all of these *CS* centers have Pr^{3+} sites of C_S symmetry, they are now labeled ''$CS(1)$'' through ''$CS(4)$,'' rather than ''$C_S(1)$'' through ''$C_S(4)$.''

The $CS(1)$ center exhibits fully reversible reorientational bleaching when excited by a linearly polarized beam. Indefinite cycles of fluorescence bleaching and recovery are possible by alternating between the two orthogonal excitation polarizations. The $CS(2)$ center exhibits partially reversible reorientational bleaching, with the intensity of the recovered fluorescence decreasing over successive cycles, accompanied by simultaneous photoproduct-formation bleaching which creates a new $CS^{\star}(2)$ photoproduct center. The $CS(3)$ and $CS(4)$ centers undergo photoproduct-formation bleaching creating the new photoproduct centers, $CS^{\star}(3)$ and $CS^{\star}(4)$, respectively. Bleaching these photoproduct centers restores the original parent centers. Models for these four Pr^{3+} centers and their bleaching behavior have already been proposed.[1] In this study, we have verified these models by detailed analysis of their polarized electronic transitions and bleaching behavior. Additional data are presented for a fifth bleachable center, henceforth labeled $CS(5)$, which plays an important role in the model assignments.

As for earlier studies, the terms ''hydrogenation'' and ''hydrogenic'' are taken to include all three hydrogen isotopes, while ''H^-'', ''D^-'', and ''T^-'' are used where necessary to specify ions of a particular isotope. Single-hydrogenic Pr^{3+} centers are formed as hydrogenic ions substitute preferentially for the interstitial charge-compensating F^- ion of an isolated Pr^{3+} center (the *A* site).[3,4] Multihydrogenic Pr^{3+} centers are derived from this C_{4v} symmetry parent center by the successive substitution of additional hydrogenic ions for the four nearest-neighbor F^- ions located between the Pr^{3+} ion and its associated charge-compensating hydrogenic ion.[1] As these hydrogenic ions are located off the C_4 symmetry axis, the Pr^{3+} site symmetry is generally reduced. In these cases γ_5 doublet states, including the $|^3H_4\Gamma_5\gamma_5\rangle$ ground state, exhibit low-symmetry crystal-

TABLE I. 10 K energy levels (in vacuum cm^{-1}, ± 0.2) measured for the $CS(1)$ through $CS(5)$ centers in deuterated SrF_2:0.05% Pr^{3+} and CaF_2:0.05% Pr^{3+}. Where they are available, the corresponding hydrogen center values are included in parentheses.

		Level				
Crystal	Center	$^3H_4(2)$	$^1D_2(1)$	$^3P_0(\gamma_1)$	$^1I_6(\gamma_1)$	$^3P_1(1)$
SrF_2	$CS(1)$	3.4(3.3)	16 706.5(6.7)	20 750.9(2.6)	20 806.9	21 236.5
	$CS(2)$	8.4(7.6)	16 612.0(1.2)	20 642.8(3.1)	20 605.7	21 104.4
	$CS(3)$	16.4(16.1)	16 566.6(4.4)	20 554.0(2.2)	20 489.0	21 011.9
	$CS(4)$	21.8(22.2)	16 667.3(5.8)	20 662.8(3.3)	20 680.3	21 142.0
	$CS(5)$		16 517.9(4.0)	20 450.4(4.5)	20 372.1	20 918.8
CaF_2	$CS(1)$	0.5	16 627.8(7.3)	20 676.9	20 585.5	
	$CS(2)$	9.6	16 530.3(29.0)	20 559.7	20 383.2	
	$CS(3)$	18.4	16 486.2(3.9)	20 463.9	20 268.1	
	$CS(4)$	19.9	16 598.5(7.0)	20 585.1	20 462.8	
	$CS(5)$		16 440.6(36.4)	20 345.0	20 151.4	

field splittings. They are all classified as *CS*-type centers. The actual Pr^{3+} site symmetries may be C_{4v}, C_{2v}, C_S, or C_1, depending on the number and locations of the substitutional hydrogenic ions.

The spectroscopy of the four major multihydrogenic Pr^{3+} centers, $CS(1)$ through $CS(4)$, has been documented for $^3H_4 \rightarrow {}^1D_2$ excitation.[1] In Sec. III we report spectral data for $^3H_4 \rightarrow {}^3P_0$ and $^3P_1$ excitation. The same fluorescence transitions, originating from the $^1D_2$ multiplet, were observed in each case. Excitation energies for the $^3H_4 \rightarrow {}^3P_0$ and $^3P_1$ absorption regions are reported for the $CS(1)$ through $CS(5)$ centers and for their $CS^{\star}(2)$ through $CS^{\star}(5)$ photoproduct centers.

The Pr^{3+} site symmetry of each *CS* center was verified by measuring polarization ratios for specific excitation and fluorescence transitions. Section IV describes how this polarization behavior was interpreted using tables of polarization ratios. Tables are presented which are appropriate for the analysis of any non-Kramers ion located in sites of C_{4v}, C_{2v}, or C_S symmetry.

The 10 K $^1D_2$ multiplet fluorescence lifetimes of the $CS(1)$ through $CS(5)$ D^- centers are reported and analyzed in Sec. V. This analysis considers the additive contribution arising from the inclusion of each successive D^- ion in the creation of these multihydrogenic centers.

Detailed polarized fluorescence bleaching and recovery sequences have been recorded to test the proposed models[1] for the $CS(1)$, $CS(2)$, and $CS(4)$ centers and the models presented in Sec. VI for the $CS(3)$ and $CS(5)$ centers. The transition intensities of the original centers and their photoproducts were measured both before and after polarized bleaching. Examples for the $CS(2)$ and $CS(5)$ centers are presented and analyzed in Sec. VII.

The thermal reequilibration behavior of the five $Pr^{3+}CS$ centers is investigated in Sec. VIII. Bleaching at 10 K creates nonequilibrium distributions of centers by reorientation and/or the creation of photoproduct centers. The temperatures at which these preferential orientations were lost and any distinct photoproducts disappeared were measured for centers in both CaF_2 and SrF_2. These temperatures are noteworthy in being essentially independent of the particular hydrogen isotope present in a given *CS* center. They also yield estimates of the barrier energies associated with the reverting processes. Some of these reequilibration results have been presented in two earlier brief accounts.[5,6]

II. EXPERIMENT

All the CaF_2:Pr^{3+} and SrF_2:Pr^{3+} crystals used in these experiments were grown by the Bridgman-Stockbarger method in a 38 kW A. D. Little R. F. induction furnace. The lowering speed was 7 mm h^{-1} for a total growth time of 18 h. The crystals were then annealed over 6 h. The starting materials were CaF_2 and SrF_2 crystal offcuts from Optovac and 99.9% pure PrF_3 powder from Alfa Inorganics. The nominal Pr^{3+} concentration was 0.05 mol % in all the crystals investigated.

The hydrogenation treatments, spectroscopic techniques, and experimental apparatus have been described for earlier spectroscopic studies of R^{3+} centers.[1,7] Hydrogenation was carried out in a 15 bar atmosphere of hydrogen gas at 900 °C for 1 h. Deuteration was performed in a $\frac{2}{3}$ bar pressure of deuterium gas at 850 °C for up to 60 h. Rhodamine 590 dye was used for laser excitation of transitions to the $^1D_2$ multiplet of Pr^{3+}, while coumarin 480 and 460 dyes were appropriate for laser excitation to the $^3P_0$ and $^3P_1$ multiplets. All the energy levels reported have been corrected for vacuum.

III. SPECTROSCOPY OF THE *CS* CENTERS

The nomenclature $^{2S+1}L_J(n)$ will be used to indicate the nth highest energy level in the multiplet $^{2S+1}L_J$. The spectroscopy of the $CS(1)$ through $CS(4)$ centers for $^3H_4 \rightarrow {}^1D_2$ excitation has already been documented.[1] A fifth center, $CS(5)$, was observed in the broadband excitation spectra of heavily hydrogenated crystals. Its transitions, while less intense than those of the other four centers, were of sufficient intensity for accurate spectroscopic characterization. $^1D_2$, ^3P_J, and $^1I_6$ energy levels were measured for all five *CS* centers and are given in Table I. These are the principal excitation energies for these centers. The $CS(1)$ through $CS(4)$ centers also have a low lying $^3H_4(2)$ energy

TABLE II. 10 K energy levels (in vacuum cm^{-1}, ± 1.0) of the $^3H_5$ and $^3H_6$ multiplets of the $CS(1)$ through $CS(5)$ centers in deuterated SrF_2:0.05% Pr^{3+}. $^3H_4$ multiplet levels have been published previously (Ref. 1).

		Center				
Multiplet	Level	$CS(1)$	$CS(2)$	$CS(3)$	$CS(4)$	$CS(5)$
	(1)	2152.6	2140.9	2135.9	2161.9	2122.8
$^3H_5$	(2)	2172.3	2149.7	2138.6	2166.8	2134.3
	(3)	2187.7	2160.4	2142.8	2173.1	
	(4)			2153.1		
	(1)	4177.5	4155.1	4135.8	4157.4	4112.6
	(2)	4181.3		4140.3	4167.0	
	(3)	4289.6				
	(4)	4483.1	4498.0	4561.1	4504.0	4600.0
$^3H_6$	(5)	4537.3	4544.9	4597.1	4557.2	
	(6)				4568.8	
	(10)	4832.7				
	(11)	4940.2	4951.4	4967.5	4942.3	4953.5
	(12)	5018.0	4972.4		4964.6	

level which is populated at 10 K. It arises from low-symmetry crystal-field splitting of the doublet $|^3H_4\Gamma_5\gamma_5\rangle$ ground state of the parent C_{4v} symmetry center, from which they are derived. Energy levels of the lowest ^3H_J multiplets were determined from fluorescence spectra. The $^3H_4$ energy levels of the $CS(1)$ through $CS(4)$ centers have been reported previously.[1] The $^3H_5$ and $^3H_6$ levels of all five *CS* centers are given in Table II. Energy levels of the $CS^\star$ photoproduct centers are given in Table III.

Laser selective excitation experiments were carried out using coumarin 480 dye to excite transitions to the $^3P_0$ multiplet, while monitoring fluorescence from the $^1D_2$ multiplet. $^3P_0$ multiplet excitation of the C_{4v} F^- center produced strong fluorescence originating from the $^3P_0$ multiplet and weak fluorescence from the $^1D_2$ multiplet. The corresponding C_{4v} D^- center had a significantly higher fraction of fluorescence from the $^1D_2$ multiplet and the C_{4v} H^- center even more. Excitation of the $^3P_0$ or $^3P_1$ multiplets of the *CS* centers produced fluorescence mostly from the $^1D_2$ multiplet. Preferential fluorescence from the $^1D_2$ multiplet for the hydrogenic centers is attributed to nonradiative relaxation from the $^3P_0$ to the $^1D_2$ multiplet, by energy transfer to the vibrational local modes of the hydrogenic ions.

TABLE III. 10 K energy levels (in vacuum cm^{-1}, ± 0.2) of the $CS^\star(2)$ through $CS^\star(5)$ photoproduct centers in deuterated SrF_2:0.05% Pr^{3+} and CaF_2:0.05% Pr^{3+}. Where they are available, the corresponding hydrogen center values are included in parentheses.

		Level		
Crystal	Center	$^3H_4(2)$	$^1D_2(1)$	$^3P_0(\gamma_1)$
SrF_2	$CS^\star(2)$	17.2(17.3)	16 664.7(4.2)	20 682.0
	$CS^\star(3)$	13.4(13.0)	16 568.7(6.9)	20 574.6
	$CS^\star(4)$	11.8(11.2)	16 676.7(5.4)	20 690.7
	$CS^\star(5)$		16 504.2(1.5)	20 483.1
CaF_2	$CS^\star(2)$	15.2	16 578.0	20 607.9
	$CS^\star(3)$	15.9	16 480.6	20 486.0
	$CS^\star(4)$	18.6	16 597.3	20 619.4
	$CS^\star(5)$			20 380.1

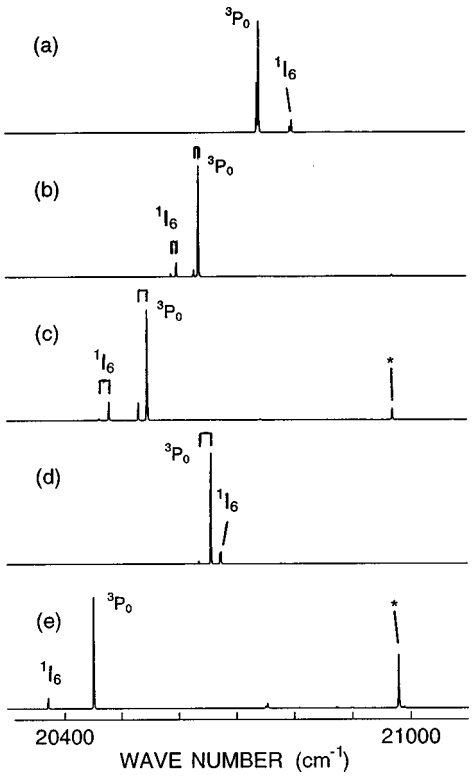

FIG. 1. 10 K selective excitation spectra of the *CS* centers in a SrF_2:Pr^{3+}:D^- crystal showing the $^3H_4 \rightarrow {}^3P_0$ and $^3H_4 \rightarrow {}^1I_6$ transitions. Spectra are for the (a) $CS(1)$ center, (b) $CS(2)$ center, (c) $CS(3)$ center, (d) $CS(4)$ center, and (e) $CS(5)$ center. The common spacings of the $^3P_0$ and $^1I_6$ line pairs show the respective $^3H_4(1)$ to $^3H_4(2)$ crystal-field splittings. The line identified by a star ($\star$) is the $^3H_4(1) \rightarrow {}^3P_0$ transition of the C_{4v} F^- center.

Site-selective excitation spectra of all five *CS* centers are presented in Fig. 1. The $CS(1)$ through $CS(4)$ centers each have a pair of transitions to the singlet $^3P_0$ level. They originate from the two levels of the crystal-field spit ground state, $^3H_4(1)$ and $^3H_4(2)$. The absence of a splitting for the $CS(5)$ center suggests that it has retained the axial symmetry of the parent center. An additional weaker pair of excitation transitions appears in each spectrum. They exhibit the same ground-state splitting, confirming that they are excitation transitions to another excited level of the selected center, probably a crystal-field state of the nearby $^1I_6$ multiplet. $^3H_4 \rightarrow {}^1I_6$ transitions are spin forbidden, but may acquire comparable intensity to the allowed $^3H_4 \rightarrow {}^3P_0$ transitions by crystal-field mixing between the $^1I_6$ and $^3P_0$ multiplets. For the C_{4v} D^- parent center in SrF_2, transitions to both the $^3P_0$ level at 20 871.1 cm^{-1} and the $^1I_6$ level at 21 052.2 cm^{-1} were observed. This identification was supported by Zeeman studies reported for the corresponding lines of the C_{4v} F^- center.[4,8] Polarization measurements on the respective excitation transitions to these $^3P_0$ and $^1I_6$ levels showed that they exhibit identical polarization behavior in each center. The $^3P_0$ level has γ_1 symmetry for all Pr^{3+} site symmetries.

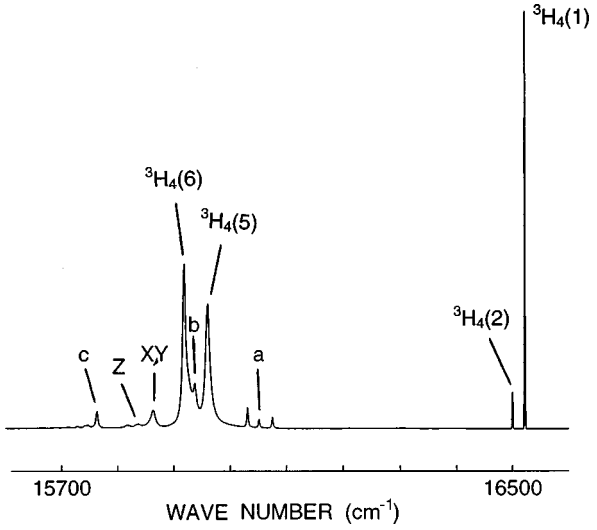

FIG. 2. 10 K fluorescence spectrum of the $CS(5)$ center in a SrF_2:Pr^{3+}:D^- crystal showing the electronic transitions from the lowest level of the $^1D_2$ multiplet to levels of the $^3H_4$ multiplet, together with the D^- vibronic transitions (*a*, *b*, *c*, *X*,*Y*, and *Z*) associated with the $^1D_2(1)\rightarrow{}^3H_4(1)$ transition.

Therefore the additional excited level is assigned as a γ_1 symmetry level of the crystal-field mixed $^1I_6$ multiplet.

Laser selective excitation experiments were also carried out using coumarin 460 dye to excite transitions to the $^3P_1$ multiplet, while monitoring fluorescence from the $^1D_2$ multiplet. For the C_{4v} D^- center, two distinct excitation transitions to the $^3P_1$ multiplet were observed. These had energies of 21 386.4 and 21 533.9 cm^{-1} in SrF_2, and 21 299.7 and 21 513.6 cm^{-1} in CaF_2. Their polarization ratios were measured and establish that these $^3P_1$ levels have γ_5 and γ_2 symmetry, respectively. The energies of the lowest $^3P_1$ energy level were also measured for the five *CS* centers in deuterated SrF_2 and these values are included in Table I.

Fluorescence spectra showing the $^1D_2\rightarrow{}^3H_4$ transitions were recorded while exciting the $^3P_0$ multiplet. The spectra of the $CS(1)$ through $CS(4)$ centers were identical to those reported previously for direct excitation of the $^1D_2$ multiplet.[1] The fluorescence spectrum of the $CS(5)$ center, for $^3P_0$ multiplet excitation, is presented in Fig. 2. Local mode vibronic transitions have been reported for the $CS(1)$ through $CS(4)$ centers.[1] From the number of transitions observed, it was concluded that the $CS(1)$, $CS(2)$, and $CS(4)$ centers have just one equivalent substitutional hydrogenic ion site each, while the $CS(3)$ center has two.[1] The new $CS(5)$ D^- center exhibits a total of five hydrogenic vibronic transitions. In deuterated SrF_2 these comprise two transitions at 659 and 686 cm^{-1}, assigned to the *X*,*Y* and *Z* modes of the interstitial charge compensating D^- ion, and three transitions at 471, 585, and 759 cm^{-1}, attributed to modes of the substitutional D^- ions. Since each substitutional ion has three vibrational modes, because of the low symmetry of these anion sites, the observation of just three transitions means that all the substitutional ions in the $CS(5)$ center must be in crystallographically equivalent sites.

All five *CS* centers exhibited fluorescence bleaching for laser excitation to their $^3P_0$ level. The $CS(1)$ and $CS(2)$ centers exhibit reorientational bleaching and the $CS(2)$, $CS(3)$, $CS(4)$, and $CS(5)$ centers exhibit photoproduct-formation bleaching, as was the case for $^1D_2$ multiplet excitation. The same photoproduct centers were produced, with excitation transitions appearing in the $^3P_0$ spectral region. As for $^1D_2$ excitation, the *CS* centers were found to bleach to an equilibrium level, with a residual fluorescence which could not be fully removed. On the other hand, it was always possible to completely revert their photoproduct centers by selective excitation.

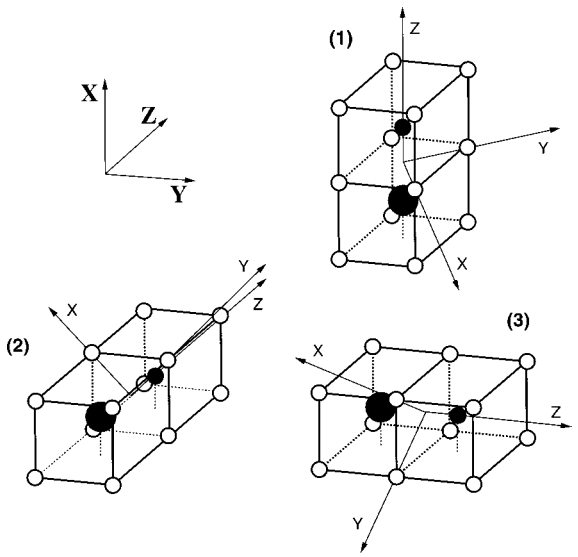

FIG. 3. The three possible orientations of a C_{4v} symmetry R^{3+} center in the fluorite lattice. This is illustrated for the C_{4v} H^- center. The crystal *X*, *Y*, and *Z* axes are also shown.

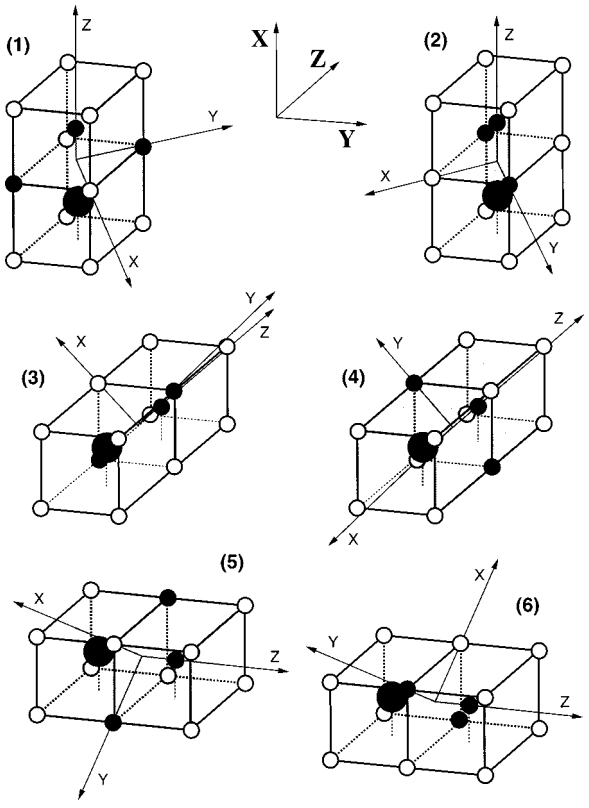

FIG. 4. The six possible orientations of a $C_{2v}(a)$ symmetry R^{3+} center in the fluorite lattice. This is illustrated for the $CS(4)$ center.

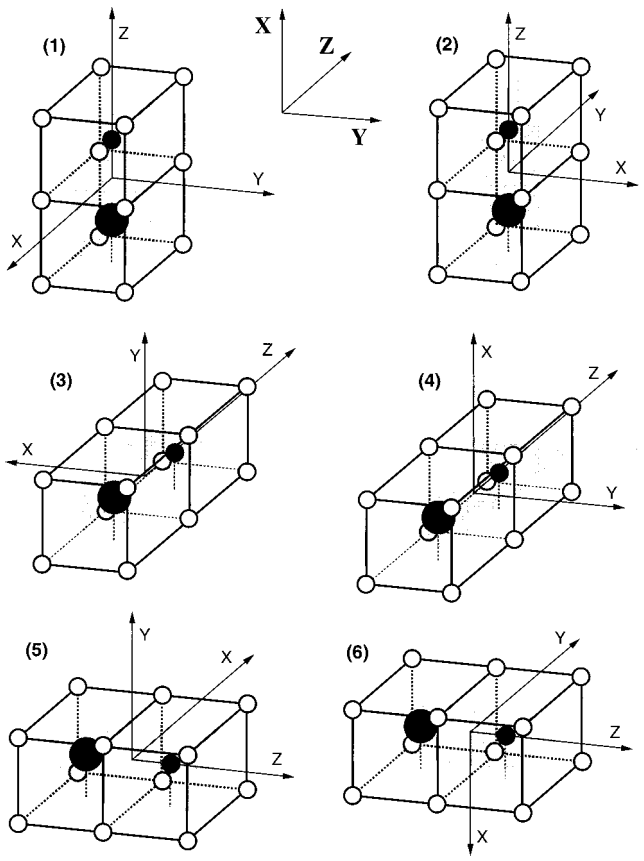

FIG. 5. The six possible orientations of a $C_{2v}(b)$ symmetry R^{3+} center in the fluorite lattice. None of the *CS* centers exhibit this symmetry.

To determine whether the excitation of bleachable centers creates photoproduct centers in the same excited state, a thorough search was conducted for any emission from the $CS^{\star}(2)$ centers during laser excitation of the parent $CS(2)$ centers. No such emission was observed. Evidently the bleaching process produces only relaxed photoproduct centers.

IV. POLARIZATION ASSIGNMENT OF Pr^{3+} SITE SYMMETRIES

The local symmetry axes of a particular center define its orientation in a crystal. The fluorite lattice has cubic symmetry, so charge compensated R^{3+} centers are distributed between at least three distinct orientations. Polarized spectroscopy helps to identify the R^{3+} site symmetries of centers[3,7,9] and to determine their distribution among the different possible orientations. The polarization geometry will be specified by $X(ab)Z$, where X is the direction of the incident laser beam, Z is the propagation direction of the fluorescence, a (Y or Z) is the plane of polarization (electric vector) of the laser beam, and b (X or Y) is the polarization of the analyzed fluorescence. The ratios of the fluorescence intensities for different combinations of a and b are called polarization ratios. The polarization ratio tables presented here for Pr^{3+} ions are equally applicable to other non-Kramers R^{3+} ions in fluorites.

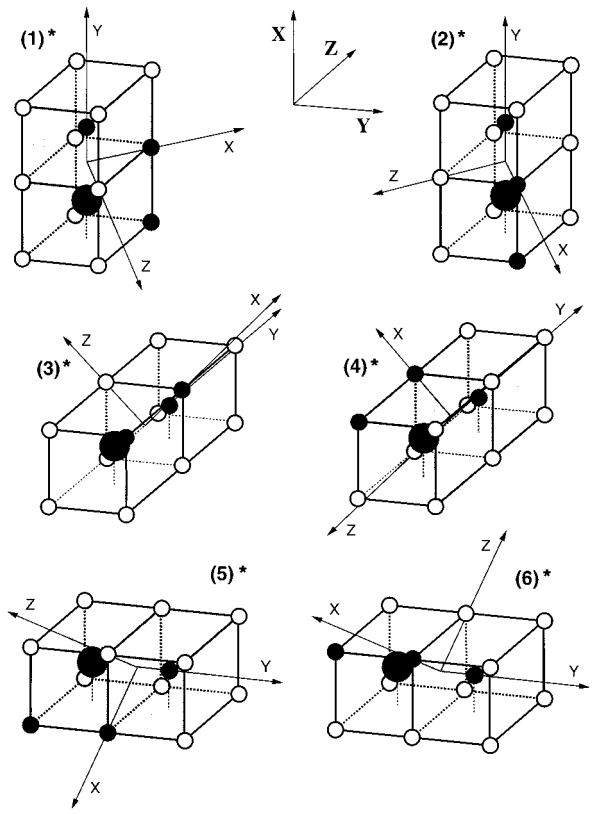

FIG. 6. The six possible orientations of a $C_S(a)$ symmetry R^{3+} center in the fluorite lattice. This is illustrated for the $CS^{\star}(2)$ center.

A. Polarization ratios for Pr^{3+} ions in sites of C_{4v}, C_{2v}, and C_S symmetry

There are three possible orientations for a C_{4v} symmetry R^{3+} center in the fluorite lattice. These are illustrated in Fig. 3 for the particular case of the C_{4v} H^- center. Each orientation has been labeled with an arbitrarily assigned number. R^{3+} centers of C_{2v}, C_S, or C_1 symmetry can be derived from the parent C_{4v} symmetry centers by anion substitutions. There are six possible ways of orienting a C_{2v} symmetry center in the fluorite lattice. In addition, two different forms of C_{2v} center, labeled $C_{2v}(a)$ and $C_{2v}(b)$, arise from the choice of the reflection plane.[9] These are illustrated in Figs. 4 and 5, respectively. Each form retains two of the four C_{4v} reflection planes, while z specifies the direction of the C_4 axis of the parent C_{4v} symmetry center. C_S symmetry centers also occur in two forms, labeled C_S (a) and C_S (b), each of which can be oriented in six different ways in the lattice.[9] These are illustrated in Figs. 6 and 7, respectively. They have a single xy reflection plane, where y specifies the C_4 axis. Different polarization ratios are obtained for the (a) and (b) forms of each symmetry.[9] For centers with no symmetry elements, having C_1 symmetry, there are 12 possible orientations: six for right- and six for left-handed C_1 symmetry centers.

By nominating the C_s symmetry reflection plane as the yz plane of the C_{4v} group, the following decomposition applies to the γ_5 irreducible representation of the C_{4v} group. It is expressed in terms of the irreps of the C_{2v} group ($\overline{\gamma}$) and the irreps of the C_S group ($\hat{\gamma}$):[10]

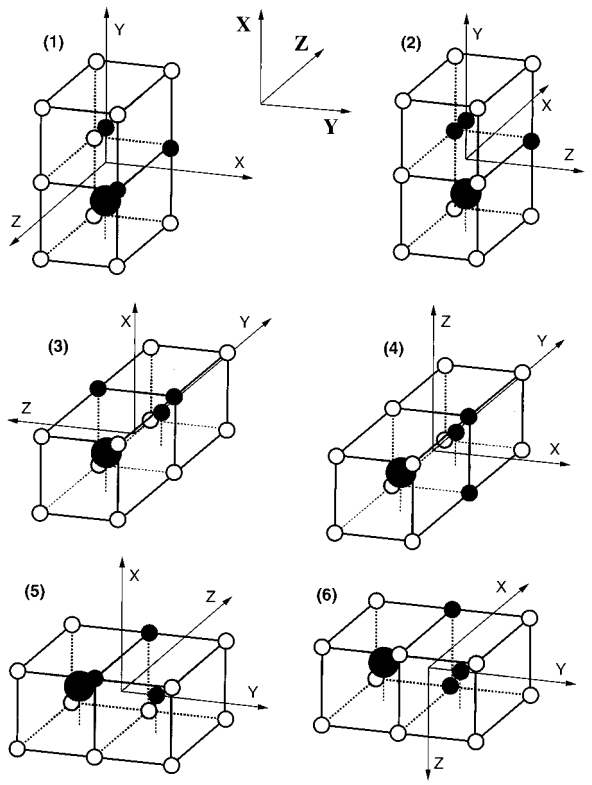

FIG. 7. The six possible orientations of a $C_S(b)$ symmetry R^{3+} center in the fluorite lattice. This is illustrated for the $CS(2)$ center.

$$\gamma_5(x,y) \rightarrow \overline{\gamma}_2(x) + \overline{\gamma}_4(y) \rightarrow \hat{\gamma}_2(z) + \hat{\gamma}_1(x \text{ or } y).$$

The two levels of a split γ_5 state have different symmetries and so transitions to or from these levels can have different polarization behavior.

The point symmetry of a R^{3+} site determines the polarizations of its R^{3+} electronic transitions. When a linearly polarized beam is aligned along one of the crystallographic symmetry axes and tuned to an absorption transition, only some orientations of that center will be excited. This orientational selectivity gives rise to polarized fluorescence spectra. It is possible to identify the R^{3+} site symmetry from the polarizations of excitation and fluorescence transitions. Detailed tables of the predicted fluorescence polarization ratios for the C_{4v}, $C_{2v}(a)$, $C_{2v}(b)$, $C_S(a)$, and $C_S(b)$ symmetry groups are presented. In an earlier study of low-symmetry mixed centers,[9] only the final fluorescence polarization ratios were presented. The extended tables given here list the relative contributions of the different center orientations, which are required to determine the Pr^{3+} site symmetries of *CS* centers and to analyze polarization bleaching sequences (Sec. VII). Although the table for $C_{2v}(b)$ symmetry is not required for any of the observed Pr^{3+} centers, it is included here for completeness.

For a given center, each electric-dipole allowed transition has a transition moment which can be resolved into its Cartesian components along the *x*, *y*, and *z* axes of that center. For excitation transitions these components of the transition moment are arbitrarily labeled *a*, *b*, and *c* for the *x*, *y*, and *z* directions, respectively. For fluorescence transitions the corresponding components are labeled *d*, *e*, and *f*. The polarization of a particular transition is specified with respect to the symmetry axes of that center. The observed polarization ratio is defined with respect to the *X*, *Y*, and *Z* axes of the host crystal and is the sum of polarized fluorescence contributions from all of the center orientations.

Non-Kramers R^{3+} ions located in sites of C_{4v} symmetry have crystal-field levels which necessarily transform as one of the five irreps of the C_{4v} point group: γ_1, γ_2, γ_3, and γ_4 are of single dimension, while γ_5 is of double dimension. The symmetries of allowed electric-dipole transitions between crystal-field levels of a C_{4v} symmetry center are[10]

C_{4v}	γ_1	γ_2	γ_3	γ_4	γ_5
γ_1	γ_1				γ_5
γ_2		γ_1			γ_5
γ_3			γ_1		γ_5
γ_4				γ_1	γ_5
γ_5	γ_5	γ_5	γ_5	γ_5	γ_1

γ_1 transitions are π (z) polarized, with the electric-field vector parallel to the C_4 axis of the site. γ_5 transitions are σ (x,y) polarized, with the electric-field vector perpendicular to the C_4 axis.

Non-Kramers R^{3+} ions in sites of C_{2v} symmetry have crystal-field levels transforming as one of the four single-dimensional irreps of the C_{2v} point group: $\overline{\gamma}_1$, $\overline{\gamma}_2$, $\overline{\gamma}_3$, and $\overline{\gamma}_4$. The symmetries of electric-dipole transitions between crystal-field levels of a C_{2v} symmetry center are[10]

C_{2v}	$\overline{\gamma}_1$	$\overline{\gamma}_2$	$\overline{\gamma}_3$	$\overline{\gamma}_4$
$\overline{\gamma}_1$	$\overline{\gamma}_1$	$\overline{\gamma}_2$		$\overline{\gamma}_4$
$\overline{\gamma}_2$	$\overline{\gamma}_2$	$\overline{\gamma}_1$	$\overline{\gamma}_4$	
$\overline{\gamma}_3$		$\overline{\gamma}_4$	$\overline{\gamma}_1$	$\overline{\gamma}_2$
$\overline{\gamma}_4$	$\overline{\gamma}_4$		$\overline{\gamma}_2$	$\overline{\gamma}_1$

$\overline{\gamma}_1$ transitions are π (z) polarized, with the electric-field vector parallel to the C_2 axis of the site. $\overline{\gamma}_2$ and $\overline{\gamma}_4$ transitions are σ_x (x) and σ_y (y) polarized, respectively, with mutually orthogonal electric-field vectors which are perpendicular to the C_2 axis.

Non-Kramers R^{3+} ions in sites of C_S symmetry have crystal-field levels transforming as one of the two single dimensional irreps of the C_S point group: $\hat{\gamma}_1$ and $\hat{\gamma}_2$. The symmetries of electric-dipole transitions between the crystal-field levels of a C_S symmetry center are[10]

C_S	$\hat{\gamma}_1$	$\hat{\gamma}_2$
$\hat{\gamma}_1$	$\hat{\gamma}_1$	$\hat{\gamma}_2$
$\hat{\gamma}_2$	$\hat{\gamma}_2$	$\hat{\gamma}_1$

Here, $\hat{\gamma}_1$ transitions may be σ_x (x) or σ_y (y) polarized, with the electric-field vector perpendicular to the C_S axis of the site. $\hat{\gamma}_2$ transitions are π (z) polarized, with the electric-field vector parallel to the C_S axis.

Fluorescence polarization ratios for each point symmetry are presented in Tables IV–VI. In these tables, the irreps of the excitation and fluorescence transitions are specified in the first and third columns, respectively. The linear polarizations

TABLE IV. Polarization ratios for C_{4v} symmetry centers in the $X(ab)Z$ geometry.

Excitation		Fluorescence		C_{4v} center orientations 1	2	3	Ratio $X:Y$
γ_5	Y			$\frac{1}{2}(a+b)$	$\frac{1}{2}(a+b)$	0	
		γ_5	X	0	$\frac{1}{4}(a+b)(d+e)$	0	
			Y	$\frac{1}{4}(a+b)(d+e)$	$\frac{1}{4}(a+b)(d+e)$	0	1:2
		γ_1	X	$\frac{1}{2}(a+b)f$	0	0	
			Y	0	0	0	1:0
	Z			$\frac{1}{2}(a+b)$	0	$\frac{1}{2}(a+b)$	
		γ_5	X	0	0	$\frac{1}{4}(a+b)(d+e)$	
			Y	$\frac{1}{4}(a+b)(d+e)$	0	0	1:1
		γ_1	X	$\frac{1}{2}(a+b)f$	0	0	
			Y	0	0	$\frac{1}{2}(a+b)f$	1:1
γ_1	Y			0	0	c	
		γ_5	X	0	0	$\frac{1}{2}c(d+e)$	
			Y	0	0	0	1:0
		γ_1	X	0	0	0	
			Y	0	0	cf	0:1
	Z			0	c	0	
		γ_5	X	0	$\frac{1}{2}c(d+e)$	0	
			Y	0	$\frac{1}{2}c(d+e)$	0	1:1
		γ_1	X	0	0	0	
			Y	0	0	0	0:0

of the excitation beam and analyzed fluorescence are specified in the second and fourth columns, respectively. The following columns give the fluorescence contributions from each center orientation, while the last column gives the net polarization ratios obtained by adding these contributions. It is assumed that all orientations are equally populated. To indicate which center orientations are excited with a given polarization geometry, the first row for each excitation polarization indicates their relative excitation probabilities. The following rows give the contribution of each center orientation to the fluorescence and the net polarization ratios.

For Z-polarized excitation, fluorescence polarization ratios are necessarily always 1:1 because the fluorescence is analyzed in the XY plane, which is symmetrical with respect to the Z axis. These entries are therefore omitted from the tables, except that for the C_{4v} center, to which specific reference is made later.

If excitation polarization ratios are required, the polarization geometry shows that they can be derived from these tables by substituting X for Z and Z for X in every instance. The net polarization ratios are then the $Z:Y$ excitation ratios. In this case, the first two pairs of columns give the irrep labels and polarization directions for fluorescence and excitation, that is in reverse order.

The C_{4v} and C_{2v} polarization ratios of Tables IV and V all reduce to numerical ratios, independent of the magnitudes of the different components of the transition moments $(a-f)$. In contrast, several of the C_S symmetry polarization ratios of Table VI do not reduce to numerical ratios and can only be evaluated with knowledge of the magnitudes of the specific excitation and fluorescence transition moments. In these cases there is a range of possible polarization ratios. For γ_1 excitation and γ_1 fluorescence of $C_S(a)$ or $C_S(b)$ symmetry centers, the polarization ratios are wholly unrestricted in range from 1:0 to 0:1. Other polarization ratios, specifically $(\frac{1}{2}a+b):a$ and $(\frac{1}{2}d+e):d$ listed for the $C_S(a)$ symmetry, are constrained in range by the requirement that all the transition moments are positive and real. For the polarization ratio $r=(\frac{1}{2}a+b)/a$, b and a are related by $2b=a(2r-1)$. Requiring both b and a to be positive and real constrains this polarization ratio to the range $r>\frac{1}{2}$. Thus, this $X:Y$ polarization ratio lies between the limits 1:0 and 1:2. Similarly, the polarization ratio $(\frac{1}{2}d+e):d$ is constrained to the same range, between 1:0 and 1:2.

All the CS centers have crystal-field levels whose wave functions are only slightly perturbed from those of the C_{4v} centers from which they are derived. It is therefore a reasonable assumption that the transition probabilities of a CS center will be little changed from those of its parent C_{4v} center. Hence, the CS center polarization ratios should closely follow those of their parent centers. This is useful for those cases where the $C_S(a)$ and $C_S(b)$ polarization ratios do not reduce to simple numerical ratios. For example, the $\hat{\gamma}_1$ symmetry ${}^3H_4(1)(\hat{\gamma}_1)\rightarrow{}^3P_0(\hat{\gamma}_1)$ excitation and $\hat{\gamma}_1$ symmetry ${}^1D_2(1)(\hat{\gamma}_1)\rightarrow{}^3H_4(1)(\hat{\gamma}_1)$ fluorescence transitions of Pr^{3+} have the ratio $(ae+bd):(2ad+2be)$ in $C_S(b)$ symmetry (Table VI). These two transitions derive from the γ_5 symmetry ${}^3H_4(1)(\gamma_5)\rightarrow{}^3P_0(\gamma_1)$ and ${}^1D_2(1)(\gamma_1)\rightarrow{}^3H_4(1)(\gamma_5)$ transitions, respectively, of the parent C_{4v} center, for which $c=f=0$. Referred to the equivalent axes of the $C_S(b)$ center, defined above, this condition becomes $b=e=0$. Hence, the polarization ratio $(ae+bd):(2ad+2be)$ be-

TABLE V. Polarization ratios for $C_{2v}(a)$ and $C_{2v}(b)$ symmetry centers.

Excitation		Fluorescence		$C_{2v}(a)$ center orientations 1	2	3	4	5	6	Ratio $X:Y$
$\overline{\gamma_1}$	Y			0	0	0	0	c	c	
		$\overline{\gamma_1}$	X	0	0	0	0	0	0	
			Y	0	0	0	0	cf	cf	0:1
		$\overline{\gamma_2}$	X	0	0	0	0	$\frac{1}{2}cd$	$\frac{1}{2}cd$	
			Y	0	0	0	0	0	0	1:0
		$\overline{\gamma_4}$	X	0	0	0	0	$\frac{1}{2}ce$	$\frac{1}{2}ce$	
			Y	0	0	0	0	0	0	1:0
$\overline{\gamma_2}$	Y			$\frac{1}{2}a$	$\frac{1}{2}a$	$\frac{1}{2}a$	$\frac{1}{2}a$	0	0	
		$\overline{\gamma_1}$	X	$\frac{1}{2}af$	$\frac{1}{2}af$	0	0	0	0	
			Y	0	0	0	0	0	0	1:0
		$\overline{\gamma_2}$	X	0	0	$\frac{1}{4}ad$	$\frac{1}{4}ad$	0	0	
			Y	$\frac{1}{4}ad$	$\frac{1}{4}ad$	$\frac{1}{4}ad$	$\frac{1}{4}ad$	0	0	1:2
		$\overline{\gamma_4}$	X	0	0	$\frac{1}{4}ae$	$\frac{1}{4}ae$	0	0	
			Y	$\frac{1}{4}ae$	$\frac{1}{4}ae$	$\frac{1}{4}ae$	$\frac{1}{4}ae$	0	0	1:2
$\overline{\gamma_4}$	Y			$\frac{1}{2}b$	$\frac{1}{2}b$	$\frac{1}{2}b$	$\frac{1}{2}b$	0	0	
		$\overline{\gamma_1}$	X	$\frac{1}{2}bf$	$\frac{1}{2}bf$	0	0	0	0	
			Y	0	0	0	0	0	0	1:0
		$\overline{\gamma_2}$	X	0	0	$\frac{1}{4}bd$	$\frac{1}{4}bd$	0	0	
			Y	$\frac{1}{4}bd$	$\frac{1}{4}bd$	$\frac{1}{4}bd$	$\frac{1}{4}bd$	0	0	1:2
		$\overline{\gamma_4}$	X	0	0	$\frac{1}{4}be$	$\frac{1}{4}be$	0	0	
			Y	$\frac{1}{4}be$	$\frac{1}{4}be$	$\frac{1}{4}be$	$\frac{1}{4}be$	0	0	1:2
				$C_{2v}(b)$ center orientations 1	2	3	4	5	6	
$\overline{\gamma_1}$	Y			0	0	0	0	c	c	
		$\overline{\gamma_1}$	X	0	0	0	0	0	0	
			Y	0	0	0	0	cf	cf	0:1
		$\overline{\gamma_2}$	X	0	0	0	0	0	cd	
			Y	0	0	0	0	0	0	1:0
		$\overline{\gamma_4}$	X	0	0	0	0	ce	0	
			Y	0	0	0	0	0	0	1:0
$\overline{\gamma_2}$	Y			0	a	a	0	0	0	
		$\overline{\gamma_1}$	X	0	af	0	0	0	0	
			Y	0	0	0	0	0	0	1:0
		$\overline{\gamma_2}$	X	0	0	0	0	0	0	
			Y	0	ad	ad	0	0	0	0:1
		$\overline{\gamma_4}$	X	0	0	ae	0	0	0	
			Y	0	0	0	0	0	0	1:0
$\overline{\gamma_4}$	Y			b	0	0	b	0	0	
		$\overline{\gamma_1}$	X	bf	0	0	0	0	0	
			Y	0	0	0	0	0	0	1:0
		$\overline{\gamma_2}$	X	0	0	0	bd	0	0	
			Y	0	0	0	0	0	0	1:0
		$\overline{\gamma_4}$	X	0	0	0	0	0	0	
			Y	be	0	0	be	0	0	0:1

comes $0:2ad$ or equivalently 0:1, in agreement with observation. These C_{4v} symmetry approximations for the C_S symmetry polarization ratios are listed in Table VII. In all cases where the polarization ratios of the parent C_{4v} center are 0:1 or 1:0, the corresponding transitions in C_S symmetry have almost the same polarization ratios.

B. Assignment of Pr^{3+} site symmetries for *CS* centers

Polarization ratios were measured with a low intensity excitation beam, with the crystal exposed for shortest duration needed to measure the fluorescence intensity. These conditions minimized bleaching and so the creation of any pref-

TABLE VI. Polarization ratios for $C_S(a)$ and $C_S(b)$ symmetry centers.

Excitation		Fluorescence		$C_S(a)$ center orientations 1	2	3	4	5	6	Ratio $X:Y$
$\hat{\gamma}_1$	Y			$\frac{1}{2}a$	$\frac{1}{2}a$	$\frac{1}{2}a$	$\frac{1}{2}a$	b	b	
		$\hat{\gamma}_1$	X	$\frac{1}{2}ae$	$\frac{1}{2}ae$	$\frac{1}{4}ad$	$\frac{1}{4}ad$	$\frac{1}{2}bd$	$\frac{1}{2}bd$	
			Y	$\frac{1}{4}ad$	$\frac{1}{4}ad$	$\frac{1}{4}ad$	$\frac{1}{4}ad$	be	be	$\frac{1}{2}ad+bd+ae:ad+2be$
		$\hat{\gamma}_2$	X	0	0	$\frac{1}{4}af$	$\frac{1}{4}af$	$\frac{1}{2}bf$	$\frac{1}{2}bf$	
			Y	$\frac{1}{4}af$	$\frac{1}{4}af$	$\frac{1}{4}af$	$\frac{1}{4}af$	0	0	$\frac{1}{2}a+b:a$
$\hat{\gamma}_2$	Y			$\frac{1}{2}c$	$\frac{1}{2}c$	$\frac{1}{2}c$	$\frac{1}{2}c$	0	0	
		$\hat{\gamma}_1$	X	$\frac{1}{2}ce$	$\frac{1}{2}ce$	$\frac{1}{4}cd$	$\frac{1}{4}cd$	0	0	
			Y	$\frac{1}{4}cd$	$\frac{1}{4}cd$	$\frac{1}{4}cd$	$\frac{1}{4}cd$	0	0	$\frac{1}{2}d+e:d$
		$\hat{\gamma}_2$	X	0	0	$\frac{1}{4}cf$	$\frac{1}{4}cf$	0	0	
			Y	$\frac{1}{4}cf$	$\frac{1}{4}cf$	$\frac{1}{4}cf$	$\frac{1}{4}cf$	0	0	1:2
				$C_S(b)$ center orientations 1	2	3	4	5	6	
$\hat{\gamma}_1$	Y			a	0	0	a	b	b	
		$\hat{\gamma}_1$	X	ae	0	0	0	bd	0	
			Y	ad	0	0	ad	be	be	$ae+bd:2ad+2be$
		$\hat{\gamma}_2$	X	0	0	0	af	0	bf	
			Y	0	0	0	0	0	0	1:0
$\hat{\gamma}_2$	Y			0	c	c	0	0	0	
		$\hat{\gamma}_1$	X	0	ce	cd	0	0	0	
			Y	0	0	0	0	0	0	1:0
		$\hat{\gamma}_2$	X	0	0	0	0	0	0	
			Y	0	cf	cf	0	0	0	0:1

TABLE VII. C_{4v} symmetry approximations to the $C_S(a)$ and $C_S(b)$ polarization ratios.

Excitation	Fluorescence	Excitation	Fluorescence	Polarization Ratio	
C_{4v} irreps		$C_S(a)$ irreps		$X:Y$	$X:Y$
γ_5	γ_5	$\hat{\gamma}_1$	$\hat{\gamma}_1$	$\frac{1}{2}ad:ad$	1:2
			$\hat{\gamma}_2$	$\frac{1}{2}af:af$	1:2
		$\hat{\gamma}_2$	$\hat{\gamma}_1$	$\frac{1}{2}cd:cd$	1:2
			$\hat{\gamma}_2$	$\frac{1}{2}cf:cf$	1:2
	γ_1	$\hat{\gamma}_1$	$\hat{\gamma}_1$	$ae:0$	1:0
		$\hat{\gamma}_2$	$\hat{\gamma}_1$	$e:0$	1:0
γ_1	γ_5	$\hat{\gamma}_1$	$\hat{\gamma}_1$	$bd:0$	1:0
			$\hat{\gamma}_2$	$b:0$	1:0
	γ_1	$\hat{\gamma}_1$	$\hat{\gamma}_1$	$0:be$	0:1
C_{4v} irreps		$C_S(b)$ irreps		$X:Y$	$X:Y$
γ_5	γ_5	$\hat{\gamma}_1$	$\hat{\gamma}_1$	$0:2ad$	0:1
			$\hat{\gamma}_2$	$af:0$	1:0
		$\hat{\gamma}_2$	$\hat{\gamma}_1$	$cd:0$	1:0
			$\hat{\gamma}_2$	$0:2cf$	0:1
	γ_1	$\hat{\gamma}_1$	$\hat{\gamma}_1$	$ae:0$	1:0
		$\hat{\gamma}_2$	$\hat{\gamma}_1$	$ce:0$	1:0
γ_1	γ_5	$\hat{\gamma}_1$	$\hat{\gamma}_1$	$bd:0$	1:0
			$\hat{\gamma}_2$	$bf:0$	1:0
	γ_1	$\hat{\gamma}_1$	$\hat{\gamma}_1$	$0:2be$	0:1

TABLE VIII. Polarization ratios for specific excitation and fluorescence transitions of the *CS* centers in a SrF_2:Pr^{3+}:D^- crystal. The *CS* center transitions are listed together with corresponding transitions of the C_{4v} D^- center from which they are derived. The calculated polarization ratios are derived in the C_{4v} approximation for the C_S symmetry $CS(1)$, $CS(2)$, and $CS(3)$ centers.

	C_{4v} D^- center transitions		*CS* D^- center transitions		Ratio $YX:YY$	
Center	Excitation	Fluorescence	Excitation	Fluorescence	Calc.	Expt.
C_{4v} F^-	$^3H_4(1)(\gamma_5)\rightarrow{}^3P_1(1)(\gamma_1)$	$^3P_0(\gamma_1)\rightarrow{}^3H_4(1)(\gamma_5)$			1:2	0.64
	$^3H_4(1)(\gamma_5)\rightarrow{}^3P_2(1)(\gamma_5)$				1:0	14.0
	$^3H_4(1)(\gamma_5)\rightarrow{}^3P_2(2)(\gamma_2)$				1:2	0.61
$CS(1)$	$^3H_4(1)(\gamma_5)\rightarrow{}^3P_0(\gamma_1)$	$^1D_2(1)(\gamma_1)\rightarrow{}^3H_4(1)(\gamma_5)$	$^3H_4(1)(\hat{\gamma}_1)\rightarrow{}^3P_0(\hat{\gamma}_1)$	$^1D_2(1)(\hat{\gamma}_1)\rightarrow{}^3H_4(1)(\hat{\gamma}_1)$	1:2	0.65
				$^1D_2(1)(\hat{\gamma}_1)\rightarrow{}^3H_4(2)(\hat{\gamma}_2)$	1:2	0.62
			$^3H_4(2)(\hat{\gamma}_2)\rightarrow{}^3P_0(\hat{\gamma}_1)$	$^1D_2(1)(\hat{\gamma}_1)\rightarrow{}^3H_4(1)(\hat{\gamma}_1)$	1:2	0.65
				$^1D_2(1)(\hat{\gamma}_1)\rightarrow{}^3H_4(2)(\hat{\gamma}_2)$	1:2	0.59
	$^3H_4(1)(\gamma_5)\rightarrow{}^3P_2(1)(\gamma_5)$	$^1D_2(1)(\gamma_1)\rightarrow{}^3H_4(1)(\gamma_5)$	$^3H_4(1)(\hat{\gamma}_1)\rightarrow{}^3P_2(1)(\hat{\gamma}_1)$	$^1D_2(1)(\hat{\gamma}_1)\rightarrow{}^3H_4(1)(\hat{\gamma}_1)$	1:0	3.94
				$^1D_2(1)(\hat{\gamma}_1)\rightarrow{}^3H_4(2)(\hat{\gamma}_2)$	1:0	6.88
			$^3H_4(2)(\hat{\gamma}_2)\rightarrow{}^3P_2(2)(\hat{\gamma}_2)$	$^1D_2(1)(\hat{\gamma}_1)\rightarrow{}^3H_4(1)(\hat{\gamma}_1)$	1:0	3.09
				$^1D_2(1)(\hat{\gamma}_1)\rightarrow{}^3H_4(2)(\hat{\gamma}_2)$	1:0	4.20
$CS(2)$	$^3H_4(1)(\gamma_5)\rightarrow{}^3P_0(\gamma_1)$	$^1D_2(1)(\gamma_1)\rightarrow{}^3H_4(1)(\gamma_5)$	$^3H_4(1)(\hat{\gamma}_1)\rightarrow{}^3P_0(\hat{\gamma}_1)$	$^1D_2(1)(\hat{\gamma}_1)\rightarrow{}^3H_4(1)(\hat{\gamma}_1)$	0:1	0.14
				$^1D_2(1)(\hat{\gamma}_1)\rightarrow{}^3H_4(2)(\hat{\gamma}_2)$	1:0	9.82
			$^3H_4(2)(\hat{\gamma}_2)\rightarrow{}^3P_0(\hat{\gamma}_1)$	$^1D_2(1)(\hat{\gamma}_1)\rightarrow{}^3H_4(1)(\hat{\gamma}_1)$	1:0	8.34
				$^1D_2(1)(\hat{\gamma}_1)\rightarrow{}^3H_4(2)(\hat{\gamma}_2)$	1:2	0.12
	$^3H_4(1)(\gamma_5)\rightarrow{}^3P_1(1)(\gamma_1)$	$^1D_2(1)(\gamma_1)\rightarrow{}^3H_4(1)(\gamma_5)$	$^3H_4(1)(\hat{\gamma}_1)\rightarrow{}^3P_1(1)(\hat{\gamma}_1)$	$^1D_2(1)(\hat{\gamma}_1)\rightarrow{}^3H_4(1)(\hat{\gamma}_1)$	0:1	0.23
				$^1D_2(1)(\hat{\gamma}_1)\rightarrow{}^3H_4(2)(\hat{\gamma}_2)$	1:0	3.08
			$^3H_4(2)(\hat{\gamma}_2)\rightarrow{}^3P_1(1)(\hat{\gamma}_1)$	$^1D_2(1)(\hat{\gamma}_1)\rightarrow{}^3H_4(1)(\hat{\gamma}_1)$	1:0	2.22
				$^1D_2(1)(\hat{\gamma}_1)\rightarrow{}^3H_4(2)(\hat{\gamma}_2)$	0:1	0.22
	$^3H_4(1)(\gamma_5)\rightarrow{}^3P_2(1)(\gamma_5)$	$^1D_2(1)(\gamma_1)\rightarrow{}^3H_4(1)(\gamma_5)$	$^3H_4(1)(\hat{\gamma}_1)\rightarrow{}^3P_2(1)(\hat{\gamma}_1)$	$^1D_2(1)(\hat{\gamma}_1)\rightarrow{}^3H_4(1)(\hat{\gamma}_1)$	1:0	3.99
				$^1D_2(1)(\hat{\gamma}_1)\rightarrow{}^3H_4(2)(\hat{\gamma}_2)$	1:0	4.52
			$^3H_4(2)(\hat{\gamma}_2)\rightarrow{}^3P_2(2)(\hat{\gamma}_2)$	$^1D_2(1)(\hat{\gamma}_1)\rightarrow{}^3H_4(1)(\hat{\gamma}_1)$	1:0	1.81
				$^1D_2(1)(\hat{\gamma}_1)\rightarrow{}^3H_4(2)(\hat{\gamma}_2)$	1:0	2.85
$CS(3)$	$^3H_4(1)(\gamma_5)\rightarrow{}^3P_0(\gamma_1)$	$^1D_2(1)(\gamma_1)\rightarrow{}^3H_4(1)(\gamma_5)$	$^3H_4(1)(\hat{\gamma}_1)\rightarrow{}^3P_0(\hat{\gamma}_1)$	$^1D_2(1)(\hat{\gamma}_1)\rightarrow{}^3H_4(1)(\hat{\gamma}_1)$	1:2	0.60
				$^1D_2(1)(\hat{\gamma}_1)\rightarrow{}^3H_4(2)(\hat{\gamma}_2)$	1:2	0.59
			$^3H_4(2)(\hat{\gamma}_2)\rightarrow{}^3P_0(\hat{\gamma}_1)$	$^1D_2(1)(\hat{\gamma}_1)\rightarrow{}^3H_4(1)(\hat{\gamma}_1)$	1:2	0.58
				$^1D_2(1)(\hat{\gamma}_1)\rightarrow{}^3H_4(2)(\hat{\gamma}_2)$	1:2	0.61
	$^3H_4(1)(\gamma_5)\rightarrow{}^3P_1(1)(\gamma_1)$	$^1D_2(1)(\gamma_1)\rightarrow{}^3H_4(1)(\gamma_5)$	$^3H_4(1)(\hat{\gamma}_1)\rightarrow{}^3P_1(1)(\hat{\gamma}_1)$	$^1D_2(1)(\hat{\gamma}_1)\rightarrow{}^3H_4(1)(\hat{\gamma}_1)$	1:2	0.62
				$^1D_2(1)(\hat{\gamma}_1)\rightarrow{}^3H_4(2)(\hat{\gamma}_2)$	1:2	0.65
			$^3H_4(2)(\hat{\gamma}_2)\rightarrow{}^3P_1(1)(\hat{\gamma}_1)$	$^1D_2(1)(\hat{\gamma}_1)\rightarrow{}^3H_4(1)(\hat{\gamma}_1)$	1:2	0.59
				$^1D_2(1)(\hat{\gamma}_1)\rightarrow{}^3H_4(2)(\hat{\gamma}_2)$	1:2	0.48
	$^3H_4(1)(\gamma_5)\rightarrow{}^3P_2(1)(\gamma_1)$	$^1D_2(1)(\gamma_1)\rightarrow{}^3H_4(1)(\gamma_5)$	$^3H_4(1)(\hat{\gamma}_1)\rightarrow{}^3P_2(1)(\hat{\gamma}_1)$	$^1D_2(1)(\hat{\gamma}_1)\rightarrow{}^3H_4(1)(\hat{\gamma}_1)$	1:0	1.39
				$^1D_2(1)(\hat{\gamma}_1)\rightarrow{}^3H_4(2)(\hat{\gamma}_2)$	1:0	1.24
			$^3H_4(2)(\hat{\gamma}_2)\rightarrow{}^3P_2(2)(\hat{\gamma}_2)$	$^1D_2(1)(\hat{\gamma}_1)\rightarrow{}^3H_4(1)(\hat{\gamma}_1)$	1:0	1.69
				$^1D_2(1)(\hat{\gamma}_1)\rightarrow{}^3H_4(2)(\hat{\gamma}_2)$	1:0	1.39

TABLE VIII. (*Continued*).

Center	C_{4v} D^- center transitions		*CS* D^- center transitions		Ratio $YX:YY$	
	Excitation	Fluorescence	Excitation	Fluorescence	Calc.	Expt.
CS(4)	$^3H_4(1)(\gamma_5)\rightarrow{}^3P_0(\gamma_1)$	$^1D_2(1)(\gamma_1)\rightarrow{}^3H_4(1)(\gamma_5)$	$^3H_4(1)(\overline{\gamma_4})\rightarrow{}^3P_0(\overline{\gamma_1})$	$^1D_2(1)(\overline{\gamma_1})\rightarrow{}^3H_4(1)(\overline{\gamma_4})$	1:2	0.58
				$^1D_2(1)(\overline{\gamma_1})\rightarrow{}^3H_4(2)(\overline{\gamma_2})$	1:2	0.61
			$^3H_4(2)(\overline{\gamma_2})\rightarrow{}^3P_0(\overline{\gamma_1})$	$^1D_2(1)(\overline{\gamma_1})\rightarrow{}^3H_4(1)(\overline{\gamma_4})$	1:2	0.58
				$^1D_2(1)(\overline{\gamma_1})\rightarrow{}^3H_4(2)(\overline{\gamma_2})$	1:2	0.57
	$^3H_4(1)(\gamma_5)\rightarrow{}^3P_2(1)(\gamma_5)$	$^1D_2(1)(\gamma_1)\rightarrow{}^3H_4(1)(\gamma_5)$	$^3H_4(1,2)(\overline{\gamma_{4,2}})\rightarrow{}^3P_2(1,2)(\overline{\gamma_{4,2}})$	$^1D_2(1)(\overline{\gamma_1})\rightarrow{}^3H_4(1)(\overline{\gamma_4})$	1:0	5.32
				$^1D_2(1)(\overline{\gamma_1})\rightarrow{}^3H_4(2)(\overline{\gamma_2})$	1:0	4.21
	$^3H_4(1)(\gamma_5)\rightarrow{}^3P_2(2)(\gamma_2)$	$^1D_2(1)(\gamma_1)\rightarrow{}^3H_4(1)(\gamma_5)$	$^3H_4(1)(\overline{\gamma_4})\rightarrow{}^3P_2(3)(\overline{\gamma_3})$	$^1D_2(1)(\gamma_1)\rightarrow{}^3H_4(1)(\overline{\gamma_4})$	1:2	0.64
				$^1D_2(1)(\gamma_1)\rightarrow{}^3H_4(2)(\overline{\gamma_2})$	1:2	0.73
CS(5)	$^3H_4(1)(\gamma_5)\rightarrow{}^3P_0(\gamma_1)$	$^1D_2(1)(\gamma_1)\rightarrow{}^3H_4(1)(\gamma_5)$	$^3H_4(1)(\gamma_5)\rightarrow{}^3P_0(\gamma_1)$	$^1D_2(1)(\gamma_1)\rightarrow{}^3H_4(1)(\gamma_5)$	1:2	0.58
		$^1D_2(1)(\gamma_1)\rightarrow{}^3H_4(3)(\gamma_1)$		$^1D_2(1)(\gamma_1)\rightarrow{}^3H_4(2)(\gamma_1)$	1:0	8.02
	$^3H_4(3)(\gamma_1)\rightarrow{}^3P_0(\gamma_1)$	$^1D_2(1)(\gamma_1)\rightarrow{}^3H_4(1)(\gamma_5)$	$^3H_4(2)(\gamma_1)\rightarrow{}^3P_0(\gamma_1)$	$^1D_2(1)(\gamma_1)\rightarrow{}^3H_4(1)(\gamma_5)$	1:0	4.30
		$^1D_2(1)(\gamma_1)\rightarrow{}^3H_4(3)(\gamma_1)$		$^1D_2(1)(\gamma_1)\rightarrow{}^3H_4(2)(\gamma_1)$	0:1	0.24
	$^3H_4(1)(\gamma_5)\rightarrow{}^3P_1(1)(\gamma_1)$	$^1D_2(1)(\gamma_1)\rightarrow{}^3H_4(1)(\gamma_5)$	$^3H_4(1)(\gamma_5)\rightarrow{}^3P_1(1)(\gamma_1)$	$^1D_2(1)(\gamma_1)\rightarrow{}^3H_4(1)(\gamma_5)$	1:2	0.59
		$^1D_2(1)(\gamma_1)\rightarrow{}^3H_4(3)(\gamma_1)$		$^1D_2(1)(\gamma_1)\rightarrow{}^3H_4(2)(\gamma_1)$	1:0	7.8
	$^3H_4(1)(\gamma_5)\rightarrow{}^3P_2(1)(\gamma_5)$	$^1D_2(1)(\gamma_1)\rightarrow{}^3H_4(1)(\gamma_5)$	$^3H_4(1)(\gamma_5)\rightarrow{}^3P_2(1)(\gamma_5)$	$^1D_2(1)(\gamma_1)\rightarrow{}^3H_4(1)(\gamma_5)$	1:0	5.14
		$^1D_2(1)(\gamma_1)\rightarrow{}^3H_4(3)(\gamma_1)$		$^1D_2(1)(\gamma_1)\rightarrow{}^3H_4(2)(\gamma_1)$	0.1	0.42
	$^3H_4(3)(\gamma_1)\rightarrow{}^3P_2(1)(\gamma_5)$	$^1D_2(1)(\gamma_1)\rightarrow{}^3H_4(1)(\gamma_5)$	$^3H_4(2)(\gamma_1)\rightarrow{}^3P_2(1)(\gamma_5)$	$^1D_2(1)(\gamma_1)\rightarrow{}^3H_4(1)(\gamma_5)$	1:2	1.02
		$^1D_2(1)(\gamma_1)\rightarrow{}^3H_4(3)(\gamma_1)$		$^1D_2(1)(\gamma_1)\rightarrow{}^3H_4(2)(\gamma_1)$	1:0	1.07

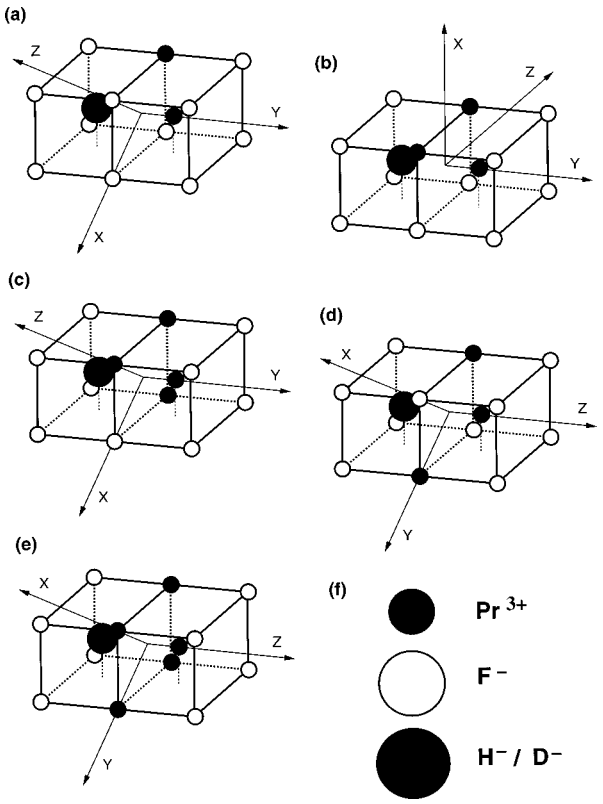

FIG. 8. The proposed ionic configurations for the (a) *CS*(1), (b) *CS*(2), (c) *CS*(3), (d) *CS*(4), and (e) *CS*(5) centers. (f) The ion spheres are drawn to the same scale as the lattice cages, to indicate their relative ionic radii.

erential center orientations. It was assumed that all center orientations were initially equally populated in crystals which had been cooled from room temperature. Each polarization ratio measurement was made on a previously unexposed section of crystal, by translating the crystal relative to the laser beam. Measured polarization ratios for all the *CS* centers in deuterated SrF_2 are presented in Table VIII and these demonstrate the range of ratios obtained.

The methodology used to deduce Pr^{3+} site symmetries is demonstrated for the *CS*(2) center. The γ_5 ground state of the C_{4v} symmetry parent center is split by 8 cm^{-1}, indicating that the Pr^{3+} site symmetry of the *CS*(2) center is lower than C_{4v}. As neither the $^1D_2(1)\rightarrow{}^3H_4(1)$ nor $^1D_2(1)\rightarrow{}^3H_4(2)$ transitions show a $X:Y$ polarization ratio of 1:2 (Table VIII), both the $C_S(a)$ and $C_{2v}(a)$ symmetries can be discounted for this center. The ratios observed are, however, consistent with either $C_S(b)$ or $C_{2v}(b)$ symmetry. The latter is also discounted as no $C_{2v}(b)$ symmetry centers can be obtained from hydrogenic ion replacements of anions in the nearest-neighbor coordination sphere of the Pr^{3+} ion. Hence, a $C_S(b)$ site symmetry is deduced for Pr^{3+} ions in the *CS*(2) center, in agreement with the previously proposed model.[1]

Polarization ratio measurements for the principal excitation and fluorescence transitions of all the *CS* centers have been presented elsewhere.[11] Similar analyses yield Pr^{3+} site symmetry assignments of $C_S(a)$, $C_S(b)$, $C_S(a)$, $C_{2v}(a)$, and C_{4v} for the *CS*(1), *CS*(2), *CS*(3), *CS*(4), and *CS*(5) centers, respectively.

TABLE IX. 10 K fluorescence lifetimes (in μs) of centers in deuterated SrF_2:0.05% Pr^{3+} and CaF_2:0.05% Pr^{3+}.

	Lifetime	
Center	SrF_2	CaF_2
C_{4v} F^-	1330±70	510±10
C_{4v} D^-	350±7	90±2
$CS(1)$ D^-	62±2	9.4±0.2
$CS(2)$ D^-	23±1	4.2±0.1
$CS(3)$ D^-	16±1	3.2±0.2
$CS(4)$ D^-	27±1	6.2±0.3
$CS(5)$ D^-	10.5±0.2	

C. Proposed models for the *CS* centers

Specific ionic configurations for the five distinct *CS* centers, consistent with their assigned Pr^{3+} site symmetries, are presented in Fig. 8. Models originally proposed[1] for the $CS(1)$, $CS(2)$, and $CS(4)$ centers all satisfy the polarization ratio constraints on their possible Pr^{3+} site symmetries and are confirmed.

It was previously reported that the $CS(3)$ center has a complex vibronic spectrum, due to the presence of at least two inequivalent substitutional hydrogenic ion sites.[1] The ionic configuration with $C_S(a)$ Pr^{3+} site symmetry illustrated in Fig. 8(c) is proposed for the $CS(3)$ center. It has three substitutional hydrogenic ions, located in two inequivalent sites between the Pr^{3+} ion and its charge-compensating interstitial ion.

The $CS(5)$ center is unusual in having a higher Pr^{3+} site symmetry of C_{4v}. Its vibronic spectrum has just five hydrogenic lines, which also indicates exact axial symmetry, with three vibronic lines associated with equivalent substitutional hydrogenic ion sites and two vibronic lines associated with the axially symmetric interstitial charge-compensating site. The ionic configuration in Fig. 8(e) is proposed for the $CS(5)$ center. It has four hydrogenic ions, located in four equivalent nearest-neighbor anion sites.

In all these proposed *CS* center models, the substitutional hydrogenic ions are located exclusively in the four anion sites between the Pr^{3+} ion and the interstitial hydrogenic ion. This constraint accounts for why just five multihydrogenic centers are observed in crystals which have not been irradiated. Further evidence for the apparent clustering of hydrogenic ions is provided by the observation that $CS(2)$ centers form preferentially to $CS(4)$ centers, although both centers contain the same number of substitutional hydrogenic ions. Clustering of hydrogenic ions is evidently favorable, to minimize the lattice strain energy of the Pr^{3+} defect centers. All the *CS* center models proposed are successful in accounting for the observed bleaching behavior under polarized excitation (Sec. VII).

V. $^1D_2$ FLUORESCENCE LIFETIMES OF THE *CS* D^- CENTERS

The 10 K fluorescence lifetimes of the lowest $^1D_2$ level were measured for all five *CS* D^- centers and the corresponding C_{4v} symmetry parent centers from which they are derived. These results are presented in Table IX. The parent

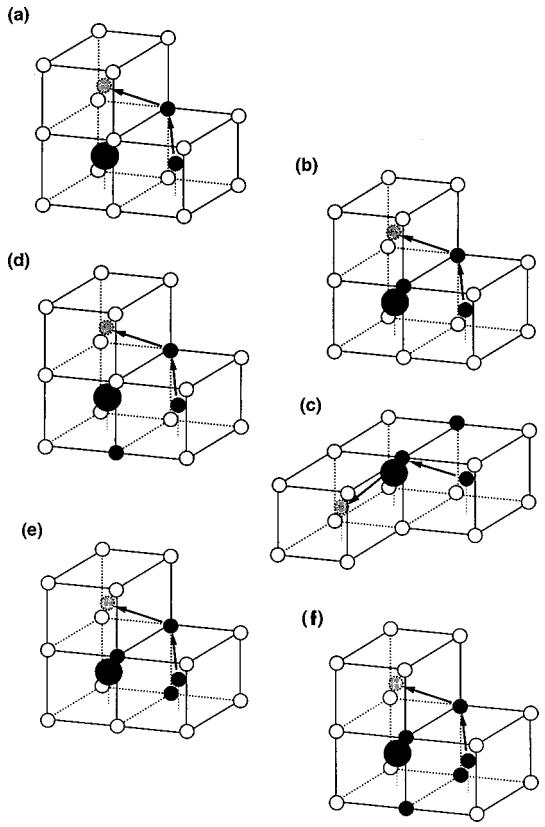

FIG. 9. The proposed mechanisms for reorientational bleaching of the (a) $CS(1)$ and (b) the $CS(2)$ centers and the proposed mechanisms for photoproduct-formation bleaching of the (c) $CS(2)$, (d) $CS(4)$, (e) $CS(3)$, and (f) $CS(5)$ centers.

C_{4v} F^- centers in both SrF_2:Pr^{3+} and CaF_2:Pr^{3+} have essentially radiative $^1D_2$ lifetimes. The corresponding C_{4v} D^- centers have shorter lifetimes, attributed to nonradiative relaxation, which is facilitated by electron-phonon coupling between the Pr^{3+} ion and the interstitial D^- ion.[3,12] Energy is transferred from the excited Pr^{3+} ion to the vibrational local modes of the D^- ion. Replacement of the D^- ion by an H^- ion further reduces the lifetime. This is due to the higher energies for vibrational modes of the lighter H^- ion.[5] Energy transfer to a higher energy mode will be a lower-order process and therefore more efficient.

As expected, the *CS* D^- centers have shorter lifetimes than their parent C_{4v} D^- centers, due to the presence of substitutional D^- ions about the Pr^{3+} ion. Efficient energy transfer is possible between the excited Pr^{3+} ion and these nearest-neighbor D^- ions. The *CS* D^- center lifetimes fall into the following series, in the order of decreasing lifetimes: $CS(1)$, $CS(4)$, $CS(2)$, $CS(3)$, and $CS(5)$. When these lifetimes are considered in terms of the models proposed for these centers in Fig. 8, it is clear that each successive substitutional D^- ion provides an additional channel for nonradiative relaxation of the Pr^{3+} ion. As these D^- ions are nearly equidistant from the Pr^{3+} ion, they should contribute equally to the nonradiative decay rate. An analysis of the *CS* D^- center lifetimes, in which each additional substitutional D^- ion contributes equally to the quenching of the Pr^{3+} fluorescence, was presented previously and strongly supports the proposed *CS* center models.[5]

VI. PROPOSED BLEACHING MECHANISMS AND MODELS FOR THE $CS^{\star}$ PHOTOPRODUCT CENTERS

The $CS^{\star}$ D^{-} centers bleach too quickly to allow a direct determination of their Pr^{3+} site symmetries by measuring polarization ratios. However, bleaching mechanisms were deduced for all of the *CS* centers from their bleaching behavior. Specific ionic configurations were thus established for the photoproduct centers observed. The models proposed for the bleaching mechanisms and the resulting photoproduct configurations are described in this section and illustrated in Fig. 9. Section VII demonstrates how these models were confirmed by detailed analysis of polarized bleaching and recovery sequences.

A general interstitialcy noncollinear mechanism[13] has already been proposed to explain the bleaching behavior observed for the $CS(1)$, $CS(2)$, and $CS(4)$ centers.[1] This involves a substitutional hydrogenic ion moving into one of the neighboring vacant interstitial sites and being replaced by the hydrogenic ion which formally occupied an interstitial site. The C_4 axis of the parent center is therefore rotated by 90°. Only the light hydrogenic ions are induced to move, limiting the possible ionic configurations which can be created. This general mechanism explained the reorientational bleaching of the $CS(1)$ and $CS(2)$ centers and the creation of a single distinct photoproduct for each of the $CS(2)$ and $CS(4)$ centers.[1] Their specific bleaching mechanisms are illustrated in Figs. 9(a), 9(b), 9(c), and 9(d), respectively.

By the same reasoning, two distinct photoproduct configurations should arise from bleaching the $CS(3)$ center, while only the one $CS^{\star}(3)$ center was observed. This result may be another manifestation of the preferential clustering of hydrogenic ions, noted previously, which favors the bleaching pathway and ionic configuration for the $CS^{\star}(3)$ center shown in Fig. 9(e). Only one photoproduct center is predicted for the $CS(5)$ center and only one was observed. The bleaching pathway and ionic configuration for the $CS^{\star}(5)$ center are shown in Fig. 9(f). Pr^{3+} site symmetries of $C_S(a)$, C_1, C_1, and $C_S(b)$ are predicted for the $CS(2)^{\star}$, $CS(3)^{\star}$, $CS(4)^{\star}$, and $CS(5)^{\star}$ centers, respectively.

VII. ANALYSIS OF POLARIZED BLEACHING SEQUENCES

When a center exhibits reorientational bleaching, particular orientations of that center can be populated preferentially through specific sequences of polarized excitation. Similarly, polarized excitation of a center which undergoes photoproduct-formation bleaching produces particular orientations of that photoproduct center. Detailed sequences of polarized bleaching were recorded and analyzed for all the *CS* D^{-} centers to test the proposed bleaching mechanisms and photoproduct configurations.[11] Two examples are presented here to demonstrate the technique and the degree of orientational selectivity which can be achieved for these multihydrogenic centers. The first is an analysis of polarized bleaching sequences for the $CS(2)$ center, which exhibits both reorientational bleaching and photoproduct-formation bleaching. The second is an analysis of the changes in polarized broadband excitation spectra as the $CS(5)$ center and its $CS^{\star}(5)$ photoproduct center are selectively bleached.

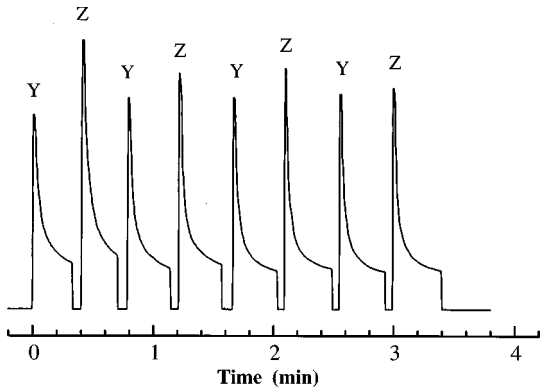

FIG. 10. A 10 K polarized bleaching sequence for the $CS(2)$ center in a SrF_2:Pr^{3+}:D^{-} crystal. The ${}^3H_4(2)\rightarrow{}^3P_0$ transition was pumped and the *X* polarized ${}^1D_2(1)\rightarrow{}^3H_4(2)$ fluorescence monitored.

A. Polarized bleaching sequences for the $CS(2)$ center

A $C_S(b)$ symmetry configuration was established for the $CS(2)$ center and its possible orientations are shown in Fig. 7. Similarly, the possible orientations of the $C_S(a)$ symmetry $CS^{\star}(2)$ center are shown in Fig. 6. Only the hydrogenic ions move during bleaching, which constrains the possible bleaching pathways. For example, consideration of Figs. 7 and 9(b) shows that only $CS(2)$ orientation 5 can be obtained by reorientational bleaching from $CS(2)$ orientation 1. Similarly, $CS^{\star}(2)$ orientations $3^{\star}$ and $4^{\star}$ in Fig. 6 are the only orientations which can be obtained by photoproduct-formation bleaching from $CS(2)$ orientation 1 in Fig. 7.

Bleaching sequences are generated by alternating between the two orthogonal excitation polarizations, *Y* and *Z*. Figure 10 shows a bleaching sequence obtained by pumping the $\hat{\gamma}_1$ symmetry ${}^3H_4(1)(\hat{\gamma}_1)\rightarrow{}^3P_0(\hat{\gamma}_1)$ transition of the $CS(2)$ center. Periods of *Y* and *Z* polarized excitation are marked on the figure. The *X*-polarized fluorescence of the $\hat{\gamma}_2$ symmetry ${}^1D_2(1)(\hat{\gamma}_1)\rightarrow{}^3H_4(2)(\hat{\gamma}_2)$ transition was monitored, so that only fluorescence from $CS(2)$ orientations 4 and 6 in Fig. 7 was observed. These are the two orientations which have their *z* axes parallel to the crystal *X* axis.

This bleaching sequence is analyzed by considering the reorientational bleaching pathways accessible for each excitation polarization. With the incident laser radiation polarized in the *Y* direction, the possible center reorientations are

$$\text{orientation } 1\rightarrow\text{orientation } 5,$$

$$\text{orientation } 4\rightarrow\text{orientation } 6.$$

With the laser radiation polarized in the *Z* direction, the possible center reorientations are

$$\text{orientation } 2\rightarrow\text{orientation } 3,$$

$$\text{orientation } 6\rightarrow\text{orientation } 4.$$

One group of $CS(2)$ centers interconverts between orientations 4 and 6 as the excitation polarization is switched between *X* and *Y*. Successive cycles of fluorescence bleaching and recovery are observed, as these are the only two orientations contributing to the observable fluorescence.

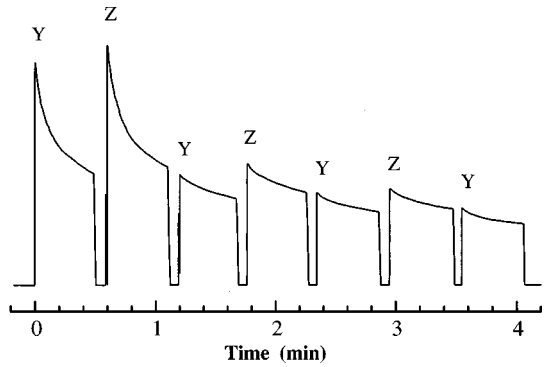

FIG. 11. A 10 K polarized bleaching sequence for the $CS(2)$ center in a $SrF_2:Pr^{3+}:D^-$ crystal. The ${}^3H_4(2)\rightarrow{}^3P_0$ transition was pumped and the X polarized ${}^1D_2(1)\rightarrow{}^3H_4(1)$ fluorescence monitored.

In the first cycle, not all the fluorescence which was bleached away during Y-polarized excitation was recovered on switching to Z-polarized excitation. Reorientational bleaching produces a redistribution of centers within the inhomogeneously broadened excitation transition.[6] Some bleached centers were pushed into the wings of the broadened transition and were no longer resonant with the excitation beam. After the first cycle, most of the $CS(2)$ centers still contributing to the observed fluorescence were those which remained resonant with the excitation beam in both orientations 4 and 6.

Figure 10 also exhibits the effects of photoproduct formation bleaching, which should produce a net decrease in the fluorescence intensity observed over multiple cycles of bleaching. This decrease was very small, indicating that reorientational bleaching is much more probable than photoproduct formation bleaching for the $CS(2)$ center.

The bleaching behavior in Fig. 10 is compared to that in Fig. 11, which was observed while pumping the $\hat{\gamma}_2$ symmetry ${}^3H_4(2)(\hat{\gamma}_2)\rightarrow{}^3P_0(\hat{\gamma}_1)$ transition of the $CS(2)$ center and monitoring the X-polarized fluorescence from the γ_1 symmetry ${}^1D_2(1)(\hat{\gamma}_1)\rightarrow{}^3H_4(1)(\hat{\gamma}_1)$ transition. In this case, only fluorescence from $CS(2)$ orientations 1, 2, 3, and 5 in Fig. 7 was observed.

With the laser radiation polarized in the Y direction, the possible center reorientations are

$$\text{orientation } 2\rightarrow\text{orientation } 3,$$

$$\text{orientation } 3\rightarrow\text{orientation } 2.$$

Excited centers interchange between orientations 2 and 3, so there is no reorientational fluorescence bleaching. With the laser radiation polarized in the Z direction, the possible center reorientations are

$$\text{orientation } 1\rightarrow\text{orientation } 5,$$

$$\text{orientation } 5\rightarrow\text{orientation } 1.$$

Again, centers are merely exchanged between orientations 1 and 5, so no reorientational bleaching can be expected. The fluorescence produced by excitation in each polarization bleaches independently because of photoproduct formation. As in Fig. 10, fluorescence may also be bleached because reorientational bleaching pushes some centers into the wings of the inhomogeneously broadened excitation transition.

This analysis of the two bleaching sequences shows that distinctive bleaching behavior is predicted for pumping $\hat{\gamma}_1$ and $\hat{\gamma}_2$ symmetry excitation transitions of the $CS(2)$ center. From the observed behavior, it is possible to make definitive irrep assignments for the ${}^3H_4(1)$ and ${}^3H_4(2)$ originating levels of the ${}^3H_4(1)\rightarrow{}^1D_2(1)$ and ${}^3H_4(2)\rightarrow{}^1D_2(1)$ transitions. The ${}^3H_4(1)$ and ${}^3H_4(2)$ levels are unambiguously identified as $\hat{\gamma}_1$ and $\hat{\gamma}_2$ states, respectively.

B. Polarized bleaching behavior of the $CS^\star(5)$ center

The $CS(5)$ center and its $CS^\star(5)$ photoproduct center have been chosen to illustrate how models for photoproduct-formation bleaching can be tested by analyzing polarized excitation spectra. The $CS(5)$ center exhibits only photoproduct-formation bleaching. With a C_{4v} symmetry configuration established for the $CS(5)$ center, its possible orientations are shown in Fig. 3. Similarly, the possible orientations of the $C_S(b)$ symmetry $CS^\star(5)$ center are shown in Fig. 7.

Figures 12(a) and 12(b) are polarized excitation spectra recorded by monitoring the broadband ${}^1D_2\rightarrow{}^3H_4$ fluorescence from both these sites. The excitation polarizations are Y and Z, respectively. After cooling the crystal from room temperature, all equivalent orientations of the $CS(5)$ center are equally populated, while the $CS^\star(5)$ center is completely absent. Inspection of Table IV shows that the γ_5 symmetry ${}^3H_4(1)(\gamma_5)\rightarrow{}^3P_0(\gamma_1)$ transition of the $CS(5)$ center should exhibit equal intensity in each excitation polarization, as observed. The integrated excitation strength is given as $a+b$ for each polarization.

Y-polarized pumping of the ${}^3H_4(1)(\gamma_5)\rightarrow{}^3P_0(\gamma_1)$ transition excites and depopulates $CS(5)$ orientations 1 and 2. Table IV shows that orientation 1 also contributes half of the absorption intensity that would be observed during Z-polarized excitation of the same transition. After this initial bleaching, the transition appeared only weakly in the Y polarization and with approximately half its initial intensity in the Z polarization, Figs. 12(c) and 12(d) respectively. This bleaching should also produce the $CS^\star(5)$ orientations $2^\star$, $3^\star$, $5^\star$, and $6^\star$ by the following conversions:

$$CS(5)\ \text{orientation } 1\rightarrow CS(5)^\star\ \text{orientations } 3^\star \text{ and } 5^\star,$$

$$CS(5)\ \text{orientation } 2\rightarrow CS(5)^\star\ \text{orientations } 2^\star \text{ and } 6^\star.$$

From Table VI, for Y-polarized excitation the $\hat{\gamma}_1$ symmetry ${}^3H_4(1)(\gamma_1)\rightarrow{}^3P_0(\gamma_1)$ transition of the $CS^\star(5)$ center has a predicted absorption strength of $2b'$. This is obtained by adding the contributions of the four photoproduct orientations created. For Z-polarized excitation the predicted strength is $2a'+b'$. As this transition is derived from the γ_5 symmetry ${}^3H_4(1)(\gamma_5)\rightarrow{}^3P_0(\gamma_1)$ transition of the C_{4v} center, for which $c=0$ and $a'>b'$ in the C_{4v} approximation, it has more intensity in the Z polarization spectrum, as observed.

The ${}^3H_4(1)(\gamma_5)\rightarrow{}^3P_0(\gamma_1)$ transition of the $CS(5)$ center was then pumped in the Z polarization, which excites and depopulates $CS(5)$ orientation 3 and further depletes orientation 1, so that only a common residual level of fluorescence

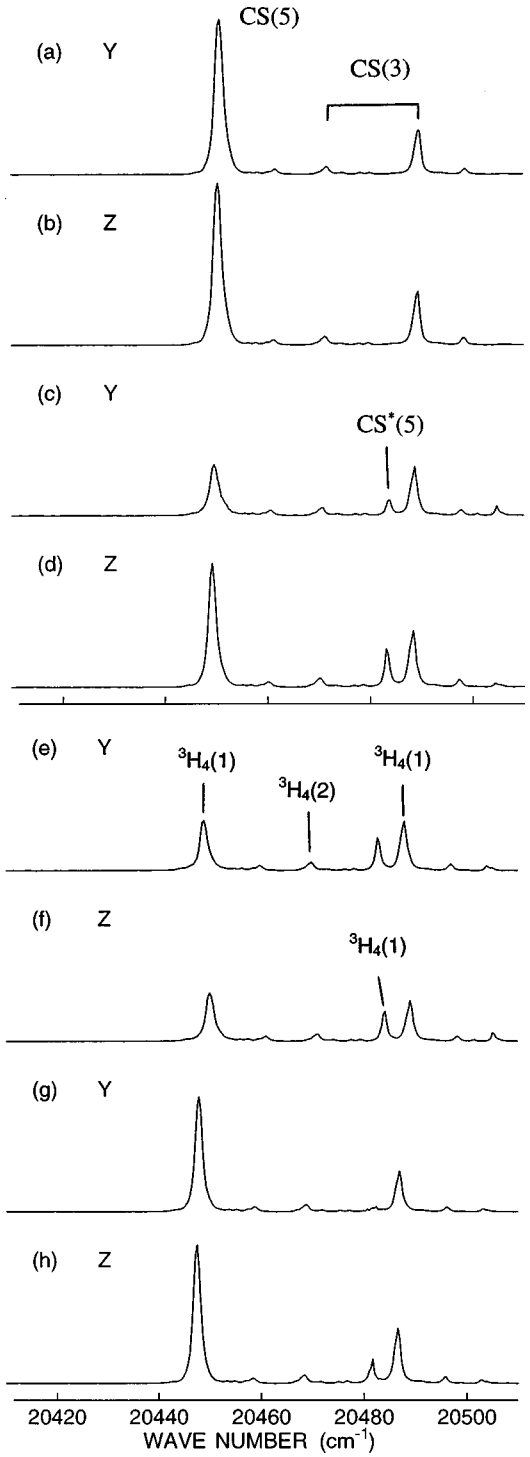

FIG. 12. A 10 K polarized bleaching sequence showing the $^3H_4(1)\rightarrow{}^3P_0$ and $^3H_4(2)\rightarrow{}^3P_0$ excitation transitions of the $CS(5)$ and $CS^\star(5)$ centers in a SrF_2:Pr^{3+}:D^- crystal. Of the following excitation spectra, (a), (c), (e), and (g) are for *Y*-polarized excitation and (b), (d), (f), and (h) are for *Z*-polarized excitation. (a) and (b) are the excitation scans prior to any bleaching, (c) and (d) were produced after *Y*-polarized pumping of the $^3H_4(1)\rightarrow{}^3P_0$ transition. (e) and (f) were produced after subsequent *Z*-polarized pumping of the same $^3H_4(1)\rightarrow{}^3P_0$ transition. (g) and (h) were produced after *Y*-polarized pumping of the $^3H_4(1)\rightarrow{}^3P_0$ transition of the $CS^\star(5)$ center.

appears in each excitation polarization, Figs. 12(e) and 12(f). This additional *Z*-polarized bleaching produces the following conversions:

$$CS(5)\ \text{orientation}\ 1\rightarrow CS(5)^\star\ \text{orientations}\ 3^\star\ \text{and}\ 5^\star,$$

$$CS(5)\ \text{orientation}\ 3\rightarrow CS(5)^\star\ \text{orientations}\ 1^\star\ \text{and}\ 4^\star.$$

As all possible orientations of the $CS(5)^\star$ center were then equally populated, the center appeared with equal intensity in the *Y* and *Z* excitation polarizations.

Finally, the $^3H_4(1)(\gamma_1)\rightarrow{}^3P_0(\gamma_1)$ transition of the $CS^\star(5)$ photoproduct center was pumped in the *Y* polarization, producing the following conversions back to the original $CS(5)$ center:

$$CS(5)^\star\ \text{orientation}\ 1^\star\rightarrow CS(5)\ \text{orientation}\ 3,$$

$$CS(5)^\star\ \text{orientation}\ 4^\star\rightarrow CS(5)\ \text{orientation}\ 3,$$

$$CS(5)^\star\ \text{orientation}\ 5^\star\rightarrow CS(5)\ \text{orientation}\ 1,$$

$$CS(5)^\star\ \text{orientation}\ 6^\star\rightarrow CS(5)\ \text{orientation}\ 2.$$

This bleaching produces a total repopulation of the $CS(5)$ orientation 3 and a partial repopulation of the $CS(5)$ orientations 1 and 2. $CS^\star(5)$ orientations $1^\star$, $4^\star$, $5^\star$, and $6^\star$ are completely depopulated. Using the tables, the *Y* polarization spectrum should have a net absorption strength of $\frac{1}{2}(a+b)$ for the $CS(5)$ center and zero intensity for the $C^\star(5)$ center. The *Z* polarization spectrum should have a net strength of $\frac{3}{4}(a+b)$ for the $CS(5)$ center and $a'+b'$ for the $CS^\star(5)$ center. This compares to the original unbleached $CS(5)$ center intensity of $a+b$ in each polarization. Polarized excitation spectra recorded after the final bleaching step, Figs. 12(g) and 12(h), show that these transitions appeared with their predicted intensities. Similar analyses have been performed for all the other bleachable centers and confirm the Pr^{3+} site symmetries and proposed bleaching mechanisms presented in Secs. IV B and VI.[11]

VIII. THERMAL RESTORATION OF *CS* CENTERS

Bleaching curves indicate how rapidly a center bleaches and these rates are a function of the bleaching efficiency, the oscillator strength of the excitation transition being pumped, and the incident laser power. Because of these factors, only relative bleaching rates have been obtained. Bleaching rates are a factor of 10 greater for hydrogen than for deuterium varieties of a given multihydrogenic Pr^{3+} center.[1,5] Bleaching rates also depend on the polarization of the excitation beam, as demonstrated by the examples of reorientational bleaching. Bleaching with linearly polarized light propagating along (100) directions produces the fastest bleaching rates, while bleaching with linearly polarized light along (110) directions or with circularly polarized light gives slower rates. In all cases, the $CS^\star$ photoproduct centers bleach more rapidly than their associated *CS* centers under the same excitation conditions.[1] Additional insight into the kinetics of bleaching has been obtained by investigating the thermal stability of the multihydrogenic centers and their photoproducts.

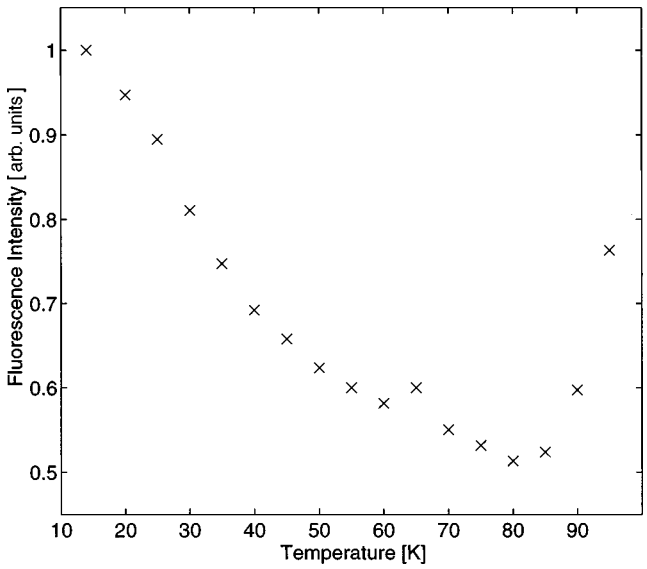

FIG. 13. Thermal restoration of the bleached $CS(2)$ center fluorescence in a $CaF_2:Pr^{3+}:D^-$ crystal, obtained by the thermal annealing technique described in the text.

A. Temperature dependences for thermal reequilibration of bleached centers

For all *CS* centers, fluorescence bleaching is permanent while the crystal is maintained at 10 K, but can be reversed by warming the crystal above 120 K.[5] The results described in this section show that restoration of any fluorescence intensity lost through bleaching occurs over a temperature range of approximately 5 K. These reverting temperatures are different for each *CS* center and are associated with a restoration of the original center configuration and the equilibrium distribution of center orientations. Two different experimental procedures were used to determine the reverting temperatures of both the hydrogen and deuterium varieties of the five *CS* centers in SrF_2 and CaF_2.

The first method was used to measure approximate reverting temperatures. Initially a given *CS* center was bleached to its residual fluorescence level, then the crystal was warmed while monitoring the fluorescence intensity at 5 K intervals. This method of ''thermal annealing'' yielded a reverting temperature defined as the lowest temperature at which a recovery of fluorescence could be clearly discerned. For the special case of the $CS(2)$ center in CaF_2, thermal reverting occurred in two steps, as shown in Fig. 13. The two reverting temperatures of 65 and 90 K correspond to the two types of bleaching exhibited by this center. Similarly, for the $CS(2)$ center in SrF_2, there was a temperature plateau around 85 K and a single step at 95 K.

More accurate reverting temperatures were obtained by the second method of ''thermal cycling,'' which has already been described in detail for the $CS(2)$ center in SrF_2.[6] After bleaching a given *CS* center, the pump beam was blocked and the crystal was warmed to a set temperature. It was held at that set temperature for 5 min before being cooled back to 10 K. This cycle was repeated for successively higher set temperatures, with the center rebleached at the beginning of each cycle. Quick exposures to the pump beam immediately before and after warming the crystal were sufficient to measure the fluorescence intensity. The degree of fluorescence recovery could thus be determined for each set temperature. These measurements could also be made on any $CS^\star$ photoproduct center to obtain the temperature at which it reverts to its original *CS* center configuration.

TABLE X. Reverting temperatures (in K) for bleached centers in $SrF_2:Pr^{3+}$ and $CaF_2:Pr^{3+}$, determined by the two methods described in the text.

Crystal	Center	Thermal annealing D^-	Thermal cycling D^-	Thermal cycling H^-
SrF_2	$CS(1)$	100±5	99±3	101±3
	$CS(2)$	85, 95±5	100±2	99±3
	$CS(3)$	75±5	80±3	79±5
	$CS(4)$	90±5	101±3	102±3
	$CS(5)$	75±5	81±3	79±5
CaF_2	$CS(1)$	85±5		
	$CS(2)$	65, 90±5	62, 90±3	66±5
	$CS(3)$	65±5	65±3	63±5
	$CS(4)$	65±5	77±2	
	$CS(5)$	60±5	66±3	

When monitoring the fluorescence recovery of a *CS* center as the crystal is cycled to successively higher set temperatures, the reverting temperature is defined as that for which $(1-1/e)$ of the bleached fluorescence is restored. For the $CS(2)$ D^- center in CaF_2, thermal reverting occurs in two steps, with these temperatures determined as 62 and 90 K. Again these correspond to the two types of $CS(2)$ bleaching. For the $CS(2)$ D^- center in SrF_2, only one recovery step could be discerned at 101 K. For the $CS(2)$ H^- centers, reverting temperatures of 66 and 99 K were measured in CaF_2 and SrF_2, respectively. Hydrogen and deuterium $CS(2)$ centers thus have equal reverting temperatures, within the estimated uncertainties.

When monitoring the waning fluorescence of a $CS^\star$ center as the crystal is cycled to successively higher set temperatures, the reverting temperature is defined as that for which the fluorescence is reduced to $(1/e)$ of its intensity immediately after bleaching the *CS* center. It was found that the $CS^\star(2)$ centers revert to the $CS(2)$ center configuration at 82 ± 3 K in SrF_2 and 56 ± 7 K in CaF_2.[6] In both cases this corresponds to the lower reverting temperature measured for the $CS(2)$ center. Reorientational bleaching is therefore associated with the higher $CS(2)$ reverting temperature.

Table X lists all the reverting temperatures measured by thermal annealing and thermal cycling. Temperatures measured by both techniques are the same within uncertainties. For any given *CS* center, reverting temperatures measured for CaF_2 were found to be lower than those for SrF_2, which may be attributed to the different lattice sizes of these crystals. In all cases, the reverting temperatures for the hydrogen and deuterium varieties of a given center are essentially the same.

B. Estimates of barrier heights from reverting temperatures

Any two ionic configurations accessible to a multihydrogenic center can be modeled as a double-well potential.[6] Bleaching involves crossing the barrier potential between

two configurations which are thermally stable in a cooled crystal. The barrier energies can be determined from the measured reverting temperatures. This has been shown previously for the case of the $CS(2)$ centers.[6] The relation used is

$$W = kT \ln(t/\tau_0),$$

where W is the barrier energy, τ_0 is the characteristic time between successive barrier crossing attempts by the mobile ions, and k is Boltzmann's constant. In the thermal cycling experiments, the crystal was held at each set temperature for a time t of 300 s. The temperature T is the reverting temperature; that for which the fluorescence recovers to $(1-1/e)$ of its intensity before bleaching. For a given value of τ_0, the measured reverting temperatures T are linearly related to the barrier energies W.

Because of their logarithmic relationship, the values obtained for W are insensitive to the particular value chosen for τ_0. For example, they vary by just 7% with a tenfold change in τ_0. Any isotopic variation of τ_0 between H^- and D^- would be undetectable given the experimental uncertainties in the measured reverting temperatures. For the chosen value for τ_0, of 10^{-12} s,[6] the barrier energy W (in cm^{-1}) is linearly related to temperature T (in K) by $W = 23.15$ T. For the measured reverting temperatures listed in Table X, the barrier energies range from 2340 ± 70 cm^{-1} for the $CS(1)$ D^- center in SrF_2 to 1530 ± 70 cm^{-1} for the $CS(5)$ D^- center in CaF_2.

C. Discussion

These barrier energies can be compared to the measured vibrational excitation energies of hydrogenic ions in *CS* centers.[1,11] For example, the interstitial D^- ion in the $CS(1)$ D^- center of SrF_2 has fundamental excitation energies ranging from 637 to 691 cm^{-1}. The substitutional D^- ion in this center has excitation energies ranging from 529 to 829 cm^{-1}. Higher energies are measured for the lighter H^- ions of the $CS(1)$ H^- center. Vibronic energies for the $CS(5)$ D^- center in SrF_2 were given in Sec. III. It is observed that generally a third-order excitation of the hydrogenic ions is required to exceed the barrier energies measured for the reverting process.

Reorientational bleaching at 10 K has never been observed for any of the C_{4v} F^-, C_{4v} H^-, or C_{4v} D^- rare-earth centers. Clearly F^- ions, which occupy all the nearest-neighbor anion sites in these centers, do not undergo light-induced migration. However, C_{4v} center reorientation has been observed at elevated temperatures by dielectric loss, EPR linewidth,[14] ionic thermal current,[15] and optical depolarization experiments.[16] Combined dielectric loss and EPR linewidth measurements yielded barrier energies for the F^-, H^-, and D^- charge-compensated centers of Gd^{3+} in CaF_2 of 3180 ± 40, 3060 ± 240, and 3470 ± 160 cm^{-1}, respectively.[14] More recent site-selective optical depolarization measurements yielded barrier energies for reorientation of the Pr^{3+} C_{4v} F^- centers in CaF_2 and SrF_2 of 3400 and 3600 cm^{-1}, respectively.[16]

Since all the multihydrogenic centers of Pr^{3+} do bleach at 10 K, the presence of at least one hydrogenic ion in a nearest-neighbor anion site is essential to the bleaching process. This supports the general interstitialcy mechanism illustrated in Fig. 9. If one of these substitutional hydrogenic ions gains sufficient vibrational energy it can move into one of the empty neighboring interstitial sites. The vacated lattice site is then filled by the excited hydrogenic ion which occupied an interstitial site in the initial configuration. This migration is probably cooperative, with both ions moving simultaneously. They will follow an equipotential path in their coordinate space as they cross over the barrier potential between the initial and final ionic configurations.[6]

The $CS(1)$ and $CS(2)$ centers have almost identical reverting temperatures, so the presence of a second substitutional hydrogenic ion does not assist the reverting process for the $CS(2)$ configuration. As some of the $CS(4)$ centers do have lower reverting temperatures, the relative locations of the substitutional hydrogenic ions appears to be important. A larger cooperative effect is found when comparing the reverting temperatures of all of the *CS* centers. The $CS(3)$ and $CS(5)$ centers have significantly lower reverting temperatures than the $CS(1)$ and $CS(2)$ centers.

Light-induced migration must involve ions which are strongly coupled to the optically active rare-earth ion. Fluorescence lifetimes are indicative of the strength of this coupling, as reviewed in Sec. V. While the Pr^{3+} C_{4v} F^- centers have essentially radiative lifetimes, the C_{4v} H^- and C_{4v} D^- centers are quenched by energy transfer to vibrational local modes of their interstitial hydrogenic ions. The multihydrogenic centers exhibit even shorter lifetimes and strong vibronic lines due to efficient electron-phonon coupling to their nearest-neighbor hydrogenic ions. Bleaching occurs in these centers because a substitutional and an interstitial hydrogenic ion can together gain sufficient vibrational energy to cross a barrier potential and create a new ionic configuration. The $CS(1)$ center in SrF_2 had the highest barrier energy, calculated as 2340 cm^{-1}. The energy gaps between the $^3P_0$ and $^1D_2$ multiplets and between the $^1D_2$ and $^1G_4$ multiplets are both approximately 3400 cm^{-1}. Hence, nonradiative relaxation between these multiplets could supply sufficient energy for barrier crossing.

IX. CONCLUSIONS

Models have been proposed for all five *CS* centers which account for their respective spectra, Pr^{3+} site symmetries, fluorescence lifetimes, bleaching behavior, and photoproduct centers. A common interstitialcy noncollinear mechanism is responsible for the bleaching of all these centers. This general model was confirmed by analyzing polarized bleaching sequences for each center.

Preferential clustering of the hydrogenic ions limits the number of possible multihydrogenic centers in a crystal cooled from room temperature to just the five *CS* centers observed. All other ionic configurations, including the $CS^\star$ centers created by bleaching, have lower barrier energies and revert to one of the *CS* configurations before the crystal reaches 10 K.

There are several reasons why the presence of hydrogenic ions in both interstitial and nearest-neighbor sites is essential for fluorescence bleaching of the multihydrogenic Pr^{3+} centers. These sites are close to the Pr^{3+} ion, so the optically active and mobile ions are strongly coupled. As the light

hydrogenic ions have comparatively high vibrational local mode energies, they can be excited efficiently by energy transfer. Sometimes they gain sufficient energy to surmount the barrier potentials between different center configurations. These barrier potentials are lower than those for the migration of lattice F^- ions. The cooperative migration of two neighboring hydrogenic ions is necessary to create a new ionic configuration which has no anion vacancies and is stable at 10 K.

ACKNOWLEDGMENTS

This research was supported by the New Zealand Lottery Board. We wish to thank R. A. Ritchie, C. H. Rowe, W. G. Smith, and R. J. Culley for technical assistance.

*Present address: Department of Chemistry, University of Wisconsin, 1101 University Ave, Madison, Wisconsin 53706. Author to whom correspondence should be addressed.

[1] R. J. Reeves, G. D. Jones, and R. W. G. Syme, Phys. Rev. B **40**, 6475 (1989).
[2] N. J. Cockroft, T. P. J. Han, R. J. Reeves, G. D. Jones, and R. W. G. Syme, Opt. Lett. **12**, 36 (1987).
[3] R. J. Reeves, G. D. Jones, and R. W. G. Syme, Phys. Rev. B **46**, 5939 (1992).
[4] B. M. Tissue and J. C. Wright, Phys. Rev. B **36**, 9781 (1987).
[5] R. J. Reeves, K. M. Murdoch, and G. D. Jones, J. Lumin. **66&67**, 136 (1996).
[6] T. Attenberger, U. Bogner, G. D. Jones, and K. M. Murdoch, J. Phys. Chem. Solids **58**, 1513 (1997).
[7] K. M. Murdoch, G. D. Jones, and R. W. G. Syme, Phys. Rev. B **56**, 1254 (1997).
[8] T. Boonyarith, J. P. D. Martin, B. Luo, and N. B. Manson, J. Lumin. **51**, 149 (1992).
[9] Y. L. Khong, G. D. Jones, and R. W. G. Syme, Phys. Rev. B **48**, 672 (1993).
[10] G. F. Koster, J. D. Dimmock, R. G. Wheeler, and H. Statz, *Properties of the Thirty-Two Point Groups* (M.I.T. Press, Cambridge, 1963).
[11] K. M. Murdoch, Ph.D. thesis, University of Canterbury, 1993.
[12] R. J. Reeves, G. D. Jones, N. J. Cockroft, T. P. J. Han, and R. W. G. Syme, J. Lumin. **38**, 198 (1987).
[13] J. Corish, C. R. A. Catlow, P. W. M. Jacobs, and S. H. Ong, Phys. Rev. B **25**, 6425 (1982).
[14] A. Edgar and H. K. Welsh, J. Phys. C **8**, L336 (1975).
[15] E. L. Kitts and J. H. Crawford, Phys. Rev. B **9**, 5264 (1974).
[16] S. P. Jamison and R. J. Reeves, J. Lumin. **66&67**, 169 (1996).